Maximum run-up produced by tsunami wave trains entering bays of variable cross section

N. Postacioglu and M. S. Özeren
Istanbul Technical University, Maslak Kampusu, 34469, Ayazaga, Istanbul, Turkey

(Received 28 July 2020; accepted 10 February 2021; published 24 March 2021)

Investigation of the behavior of various types of tsunami wave trains entering bays is of practical importance for coastal hazard assessments. Furthermore, a mathematical algorithm for quick analysis of the run-up in bays for a large number of incident wave scenarios is also a practical need for tsunami hazard assessments. The linear shallow water equations admit two types of solutions inside an inclined bay with parabolic cross sections: energy-transmitting modes and modes with spatial decay towards the inland tip of the bay. In the low-frequency limit there is only one mode susceptible of transmitting energy to the inland tip. A full solution for the run-up requires taking into account these two types of modes and the scattered field outside, leading to mathematical complications. However, in the long wave limit, this complication can be avoided if one imposes the free surface at the bay mouth being equal to twice the disturbance associated with the incident wave in the open sea. The run-up produced by the solution obtained from this Dirichlet boundary condition can be easily calculated using a series of images. In this model no energy is allowed to escape from the bay; therefore the error arising from the simplification of the boundary condition at the bay mouth grows with time. Nevertheless the maximum run-up occurs before this error becomes significant. If the standard deviation of a Gaussian-shaped incident wave is 8 times the square root of the width of the bay, then this simple solution overestimates the first maximum of the run-up only by 12% compared to the exact solution calculated by means of an integral equation. This overestimation is partly due to the fact that the Dirichlet boundary conditions violate the continuity of the fluxes at the bay mouth. The solution associated with the Dirichlet boundary condition is perturbed in order to match fluxes inside and outside of the bay. The height of the first maximum of the run-up coming from the perturbation theory is in excellent agreement with the "exact" solution. This perturbation theory can also be applied to narrow bays with an arbitrary cross section as long as their depth does not change significantly in the longitudinal direction. The method developed here can also be used to calculate maximum run-up in noninclined bays of arbitrary cross section.

DOI: 10.1103/PhysRevFluids.6.034803

I. INTRODUCTION

Waves grow as they approach a shoreline due to the decreasing water depth (see Ref. [1]). This is valid for all shoaling bathymetries and is even more pronounced in converging bays. An early relevant mathematical study of waves in bays of varying cross sections was done in Ref. [2] (see article 185–186 in the book, pp. 275–278). More recently Ref. [3] used the WKB-based approach to calculate transmission and reflection coefficients for a channel of variable cross section. The behavior of waves in the vicinity of shoreline has been an active research topic for a long time [4–6]. Most of these analytical and numerical models consider a wave train of various shapes progressing first over a flat ocean and then making a passage over a sloping bathymetry leading to a beach. Let

us look at the one-dimensional version of the problem, which has important practical applications in the context of tsunamis and storm surges. An obvious difficulty for both analytical and numerical studies is the nature of the open boundary condition offshore. The reason that this is difficult is that after a certain time the waves will start getting reflected from various features of bathymetry and the shoreline itself. Since this reflecting wave field is unknown at the offshore boundary, it is not clear how to pose the boundary value problem. To overcome this difficulty, Ref. [7] turned this into an initial value problem where they imposed the value of the free surface at the offshore boundary point in a particular way in which it remained equal to twice that of the vertical displacement of the free surface generated by the incident wave arriving from the open sea. In the rest of this article we will refer to this as the Dirichlet boundary condition. They also assumed an initially flat and quiet free surface between the offshore boundary and the shoreline. They then calculated the nonlinear wave evolution subject to this boundary condition at all times. In this, they observed a strong resonant regime. Indeed, such a resonance has been confirmed in later studies [8–10] in the presence of uneven bathymetries. These studies mentioned above used radiation conditions offshore, implemented in various ways so that no prescription of a boundary condition at a particular point was necessary to cast the problem. In this work, we will show that a boundary condition offshore with the free surface itself being prescribed [7] at a single point can be used to calculate run-up, at least for a limited timescale that characterizes tsunami phenomena for certain geometric settings including narrow nonreflecting bays bordering a flat ocean bed. Waves near bay mouths often have complex patterns, and they are often mathematically handled using conformal mappings provided that the depth variation is small in this region [10–12]. Some nonreflecting geometries such as sloping bays with a parabolic cross section cannot be approached by this class of analytical means. This is because the depth spans all values along the mouth of the bay. In this study we will determine the cases where a simple Dirichlet condition at a single point offshore is good enough to study the run-up characteristics for tsunami-like incident waves for all bay geometries that we consider in this work. The boundary value problem cast in this manner has the advantage of rendering the problem one-dimensional within the bay. We will compare these one-dimensional solutions with full two-dimensional ones featuring far-field radiation conditions. In the literature there are a number of studies examining wave propagation and run-up in converging bays but none considering the scattering of the incident wave by the mouth of the bay (see Refs. [13,14] and [15–18]) Furthermore we investigate the perturbed version of the one-dimensional approach with the expansion parameter being the width of the bay divided by the dominant wavelength of the incident wave. The purpose of this asymptotic perturbation approach is to handle the radiation damping that stems from the nonvanishing width of the bay. We show that it is possible to do this while keeping the computations one-dimensional within the bay.

In the next section we will first start with a simple case where there is just a bathymetric step with the domain having an infinite width. The reason we study this simple case is that the resulting run-up shows all the main characteristics run-ups occurring in the bays. For this one-dimensional case the solution of the linear shallow water equation for an arbitrary incident wave can simply be written as a geometric series.

Next, we consider a nonsloping rectangular bay for which there is no closed form solution. To remedy this we develop a solution based on an integral equation. All noninclined bays are obviously nonreflecting. As a first nontrivial case of a nonreflecting inclined bay we consider the case of parabolic cross section. We derive a dispersion relation (for both real and imaginary wave vectors) valid for noninclined *channels* of parabolic cross section and use it to solve an integral equation at the mouth of the inclined bays of the same type of cross section. The waves associated with the purely complex wave vectors decay rapidly towards the tip of the bay, hence they are not influenced by the slope. We use these decaying modes to solve the integral equation at the mouth of the bay. The integral equation approach is numerically heavy, unlike the above-mentioned asymptotic method. The result from the integral equation is compared with those from the asymptotic expansion.

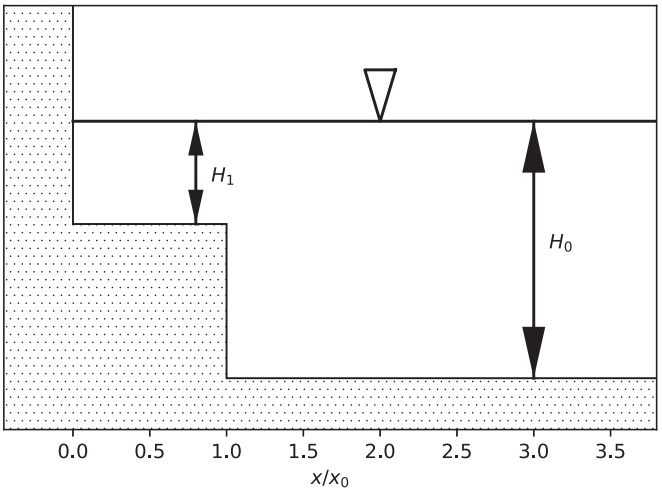

FIG. 1. The bathymetry of the laterally infinite case featuring a coastal wall, a shallow shelf connecting to an infinite ocean with a flat bottom. Here $x = 0$ is the shoreline, and $x = x_0$ is the position of the toe. The depth of the shallow shelf is H_1, and the depth of the open sea is H_0.

II. INCIDENT WAVES APPROACHING AN INFINITELY WIDE SHELF WITH STEPLIKE BATHYMETRY

When a normally incident wave approaches an infinitely wide shelf connecting to a deep ocean with flat bathymetry, some energy gets transmitted onto the shallow shelf. According to linear shallow water (LSW) equations the ratio between the transmitted energy and the incident wave's total energy is independent of the wavelength with the transmission coefficient being equal to $2\frac{\sqrt{H_0}}{\sqrt{H_0}+\sqrt{H_1}}$ (see Ref. [11], p. 119). Here H_0 and H_1 are the depths of the open ocean and shelf, respectively (see Fig. 1). This transmitted wave gets completely reflected by the shoreline and arrives at the toe and gets reflected from there again with the reflection coefficient $\frac{\sqrt{H_1}-\sqrt{H_0}}{\sqrt{H_1}+\sqrt{H_0}}$, which is negative. The resulting wave field over the shelf can be written as

$$\eta(t,x) = 2\frac{\sqrt{H_0}}{\sqrt{H_0}+\sqrt{H_1}}\left[\sum_{k=0}^{\infty}\epsilon^k\eta_{\text{inc}}\left(t-\frac{x_0-x}{\sqrt{gH_1}}-2k\frac{x_0}{\sqrt{gH_1}},\ x_0\right)\right.$$
$$\left.+\epsilon^k\eta_{\text{inc}}\left(t-\frac{x}{\sqrt{gH_1}}-(2k+1)\frac{x_0}{\sqrt{gH_1}},\ x_0\right)\right], \tag{1}$$

where g is acceleration due to gravity and ϵ is given as

$$\epsilon = \frac{\sqrt{H_1}-\sqrt{H_0}}{\sqrt{H_1}+\sqrt{H_0}}.$$

Here the wave field is expressed as a function of the value the incident wave takes at the toe. If we take the limit $H_0 \to +\infty$, the above series reduces to $2\eta_{\text{inc}}(t, x_0)$ for $x \to x_0^-$; in other words, the Dirichlet boundary condition as stated in Ref. [7] is satisfied.

When H_0 is large but finite, the above-mentioned Dirichlet condition will remain valid only for a limited amount of time. To calculate the length of time for which the Dirichlet condition is valid, consider an incident wave of the following form:

$$I_0\theta[\sqrt{gH_0}t+(x-x_0)]\sin\left[\omega\left(t+\frac{x-x_0}{\sqrt{gH_0}}\right)\right], \tag{2}$$

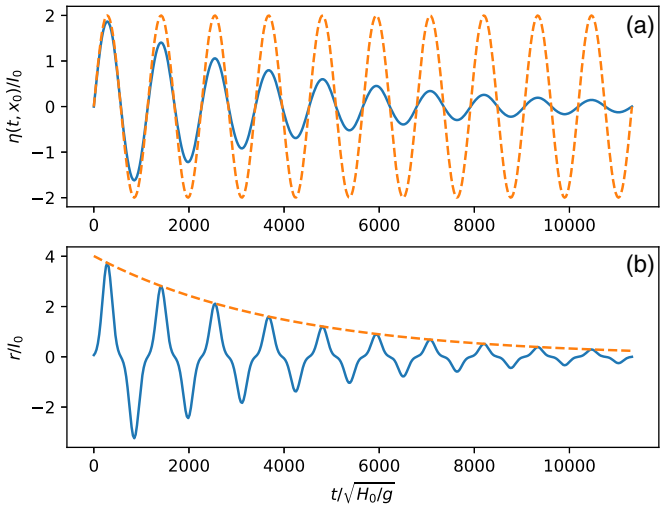

FIG. 2. Incident wave approaching a shallow shelf of infinite width. (a) The continuous curve is the normalized free surface disturbance at $x = x_0$ (the toe of the slope) for an incident wave given by (2). The frequency, ω, of the incident wave is $\sqrt{gH_1}\pi/(2x_0)$ and $x_0/H_0 = 20$. The ratio, H_0/H_1, is 200. The broken curve is twice the amplitude of the incident wave at the toe. (b) The continuous curve is the time evolution of the normalized run-up for an incident wave of Gaussian shape given by $I_0 \exp\left[-4\frac{gH_1}{x_0^2}\left(t + \frac{x-x_0}{\sqrt{gH_0}}\right)^2\right]$ for the same bathymetry as (a). The dashed curve is the decay envelope given by $(r_{\max}/I_0)\exp\left[-|\mathrm{Im}\omega_k|(t - t_{\max})\right]$, where ω_k is a natural frequency of the radiating mode given in Eq. (5). Note that the imaginary part of the frequencies of all modes is equal. For both panels the width is infinite.

where θ is the step function ($\theta(x) = 1$ if $x > 0$ and else it is zero. Note that this incident wave reaches the toe at $t = 0$. If we substitute (2) in Eq. (1) we obtain the time evolution of the wave given in Fig. 2(a). It is easy to see that the major part (almost all) of the energy of the incident wave will be reflected back at $x = x_0$, which is the toe of the shallow shelf. This is due to the very large depth contrast and the toe acting almost like a solid vertical wall. Note here that the transmitted power of a linear shallow water wave at any given point is equal to $Hu\rho g\eta$ where H, u, ρ, and η are water depth, fluid velocity, water density, and the free surface vertical displacement, respectively. Hence, at the toe, the depth-averaged fluid velocity being almost zero, only a very small part of the power is transmitted onto the shelf. This means that the incident and reflected waves will be superimposed at $x = x_0^+$, leading to an oscillation with amplitude equal to $2I_0$ there. This oscillation will trigger a progressive wave towards the shore with amplitude $2I_0$. This wave will be reflected from the shoreline and will arrive back to the toe. There a tiny part of it will be transmitted onto the open ocean, and the amplitude of this will be

$$\frac{4I_0\sqrt{H_1}}{\sqrt{H_0} + \sqrt{H_1}} \ll 2I_0. \tag{3}$$

Therefore the perturbation of the offshore boundary condition will be negligible. The process will continue, setting up a standing wave regime over the shelf, with an amplitude increasing with time (until the steady regime is reached due to the wave radiation into the open sea) because the incident wave will keep arriving. Although only a tiny percentage of this standing wave will create a transmission towards offshore, it too will increase with time and may become of the same order of $2I_0$, therefore rendering the Dirichlet boundary condition at the toe invalid.

For a monochromatic incident wave with a frequency matching the first resonant frequency of the shallow shelf [$\omega_1 = \sqrt{gH_1}\pi/(2x_0)$], it can easily be shown that the *standing* wave solution is

given as

$$\eta(t,x)=\begin{cases}2I_0\sqrt{H_0/H_1}\cos\left(\frac{\pi}{2x_0}x\right)\sin(\omega_1 t) & \text{for} \quad 0<\mathrm{x}<\mathrm{x}_0\\ 2I_0\sin\left[\frac{\pi}{2x_0}\sqrt{\frac{H_1}{H_0}}(x-x_0)\right]\sin(\omega_1 t) & \text{for} \quad \mathrm{x}>\mathrm{x}_0.\end{cases} \tag{4}$$

The second line of the above formula corresponds to the superposition of the incident wave and the reflected wave, thus indicating radiation towards the open ocean. This particular standing wave solution maintains $\eta=0$ at the toe during the steady regime. The transient (1) before this steady regime sets in is shown in Fig. 2(a). In both panels of Fig. 2, one notices that the elapsed time between two consecutive maxima is four times the travel time of the wave between the toe and the coastal wall. This is because the wave changes polarity only at the reflections at the toe.

To calculate the time necessary to reach the standing wave state, note first that the standing wave above does not satisfy the initial conditions, $\eta(t=0,x)=0$, $\partial_t\eta(t=0,x)=0$ over the shallow shelf. Therefore the temporally decaying solutions of the homogeneous wave equation (not driven by the incident wave) need to be added to it. The decay time of these homogeneous solutions is the time necessary to reach the standing wave regime. Any wave corresponding to the homogeneous solution, traveling on the shallow shelf, when reflected by the toe of the shelf gets its amplitude multiplied by $1-2\sqrt{H_1/H_0}$ for $H_1\ll H_0$. The polarity is reversed each time such a reflection occurs simply because the direction of propagation goes from shallow to the deep. Such consecutive weak damping at the toe will erode the wave exponentially, leading to a wave proportional to $\exp\left[t\ln\left(1-2\sqrt{\frac{H_1}{H_0}}\right)/(2x_0/\sqrt{gH_1})\right]$, which approximately simplifies to $\exp\left[-t\ 2\sqrt{\frac{H_1}{H_0}}/(2x_0/\sqrt{gH_1})\right]$. Here $(2x_0/\sqrt{gH_1})$ is the two-way travel time of the wave over the shallow shelf. Now let us elaborate on the spatial and oscillatory behavior of these homogeneous solutions. These decaying solutions satisfy usual boundary conditions at the toe (continuity of the free surface and that of the depth-integrated velocity). These homogeneous solutions transmit energy in the offshore direction. All these conditions can be satisfied at certain complex frequencies given by

$$\omega_n=\frac{\sqrt{gH_1}}{x_0}\left[\frac{\pi}{2}+n\pi+i\tanh^{-1}\left(\sqrt{H_1/H_0}\right)\right],\quad n=0,1,2,\ldots, \tag{5}$$

where $\tanh^{-1}\sqrt{H_1/H_0}$ can be approximated by $\sqrt{H_1/H_0}$. Hence the decay time is approximately $(x_0/H_1)\sqrt{H_0/g}$ [see Fig. 2(b)]. The explicit form of these solutions is

$$\eta(t,x)=\begin{cases}\cos\left(\frac{\omega_n}{\sqrt{gH_1}}x\right)\exp(i\omega_n t) & \text{for} \quad 0<\mathrm{x}<\mathrm{x}_0\\ \cos\left(\frac{\omega_n}{\sqrt{gH_1}}x_0\right)\exp\left[i\omega_n\left(t-\frac{x-x_0}{\sqrt{gH_0}}\right)\right] & \text{for} \quad \mathrm{x}>\mathrm{x}_0.\end{cases} \tag{6}$$

According to the linear theory, the Fourier transform of the run-up is the Fourier transform of the incident wave at a given point multiplied by the response function. The natural frequencies of the homogeneous solutions are the poles of this response function in the complex ω-plane. The response function for various geometries is given in Refs. [4,9,10].

Two animations have been produced in order to visualize the incident sinusoidal wave and Gaussian wave train (see the Supplemental Materials [19] and [20]). Our discussion so far involved neither a bay nor a sloping bathymetry. The reason we investigated a simple step bathymetry so far is that it has significant relevance for nonreflecting bays where, once a wave enters it, the energy is transmitted all the way to the inland tip and reflects only from there. In Ref. [21] it was shown that inclined bays of parabolic cross section satisfy this condition.

A. Rectangular bay of uniform depth

In this section we will look at the wave behavior within rectangular bays of uniform depth when the dynamical source is an incident wave. Any noninclined bay is obviously nonreflecting, and this

is the simplest possible case where we can initiate our discussion and eventually cover inclined nonreflecting bays. Consider now a rectangular bay of width $2Y_0$ of uniform depth H opening to a sea of the same depth. If we apply the Dirichlet condition of $\eta(t, x_0^- 1) = 2\eta_{\text{inc}}(t, x_0^+)$ at the toe of the bay, the problem becomes one-dimensional, and the solution within the bay can be obtained from (1) where H_1 will be replaced by depth H and H_0 by ∞. When H_0 is taken to be ∞ the Dirichlet condition automatically becomes valid, and the fluid velocity in the x direction becomes essentially zero for $x = x_0^+$. But this is not the case at $x = x_0^-$ because when the incident wave hits the bay mouth, a progressive wave is triggered inside the bay. Our aim here is to find a scattered field outside such that the continuity of both u and η is maintained. We propose the following solution for the entire bay:

$$\eta(t,x) = \int_0^\infty d\omega \left\{ B_0(\omega)\cos\left(\frac{\omega}{\sqrt{gH}}x\right)\exp(i\omega t) + \sum_{n=1}^{N} B_n(\omega)\frac{\cosh[\sqrt{gH(n\pi/Y_0)^2-\omega^2}\,x/\sqrt{gH}]}{\cosh[\sqrt{gH(n\pi/Y_0)^2-\omega^2}\,x_0/\sqrt{gH}]}\cos\left(\frac{n\pi}{Y_0}y\right)\exp(i\omega t) + \text{c.c.}\right\}, \quad (7)$$

where the first term is an oscillatory solution of the one-dimensional linear wave equation that satisfies the no-flux condition at the coastal wall ($x = 0$). There is only one oscillatory mode in the x direction if ω^2 is smaller than $gH(\pi/Y_0)^2$. The rest of the integrand corresponds to a two-dimensional solution of the wave equation that decays exponentially in the $-x$ direction. This decaying solution also satisfies no-flux condition in the side walls $y = \pm Y_0$. The solution given above is symmetrical with respect to $y = 0$. For narrow bays ($\omega/\sqrt{gH} \ll 1/Y_0$) the ratio of the hyperbolic cosines approximately becomes $\exp[\sqrt{gH(n\pi/Y_0)^2-\omega^2}\,(x-x_0)/\sqrt{gH}]$. The y-dependence is simply $\cos(\frac{n\pi}{Y_0}y)$ with $n = 1, 2, 3, \ldots$. The reason for the discrete summation over the positive integers is that the y-dependent part of the solution is eigenfunctions of the operator $\frac{d^2}{dy^2}$ satisfying the von Neumann condition ($\partial_y\eta = 0$) at $y = \pm Y_0$. As we will see, finding the eigenfunctions for the case of parabolic cross sections will not be trivial. The coefficients B_n in the above expression will be calculated using the boundary conditions at the mouth of the bay.

If the incident wave train is $\int_0^\infty d\omega I_0(\omega)\exp[i\omega(x-x_0)/\sqrt{gH}]\exp(i\omega t) + \text{c.c.}$, then the sum of incident, reflected, and scattered wave will be

$$\eta^{\text{open}}(t,x,y) = \int_0^\infty \left\{ 2I_0(\omega)\cos\left[\frac{\omega}{\sqrt{gH}}(x-x_0)\right]\exp(i\omega t) + \left[\frac{\omega}{2gH}\int_{-Y_0}^{Y_0} dy^*\,\tilde{s}(\omega,y^*)\mathrm{H}_0^{(2)}\left(\frac{\omega}{\sqrt{\mathrm{gH}}}|\mathbf{r}-\mathrm{x}_0\hat{\mathbf{i}}-\mathrm{y}^*\hat{\mathbf{j}}|\right)\exp(\mathrm{i}\omega\mathrm{t})\right] + \text{c.c.}\right\} \mathrm{d}\omega \quad (8)$$

in the open sea. Here $\mathrm{H}_0^{(2)}$ is the zeroth-order Hankel function of the second kind [see Ref. [22], formula (9.1.4)]. The scattered wave progresses in the outward direction in the far field ($\omega|\mathbf{r} - x_0\hat{\mathbf{i}} - y^*\hat{\mathbf{j}}| \gg gH$) because the Hankel function $\mathrm{H}_0^{(2)}(\mathrm{z})$ is proportional to $\exp(-iz)$ for large z. Function $\tilde{s}(\omega, y^*)$ in Eq. (8) is the temporal Fourier transform of the virtual sources placed at the mouth of the bay. These sources will ensure the continuity of the fluid flow across the mouth. The depth-integrated flow associated with $\frac{\omega}{2gH}\mathrm{H}_0^{(2)}(\frac{\omega}{\sqrt{\mathrm{gH}}}|\mathbf{r}-\mathrm{x}_0\hat{\mathbf{i}}-\mathrm{y}^*\hat{\mathbf{j}}|)\exp(\mathrm{i}\omega\mathrm{t})$ is the gradient of it multiplied by igH/ω. The gradient of $\frac{i}{2}\mathrm{H}_0^{(2)}(\frac{\omega}{\sqrt{\mathrm{gH}}}|\mathbf{r}-\mathrm{x}_0\hat{\mathbf{i}}-\mathrm{y}^*\hat{\mathbf{j}}|)$ for small arguments approximately reads

$$\frac{1}{\pi}\frac{\mathbf{r}-x_0\hat{\mathbf{i}}-y^*\hat{\mathbf{j}}}{\left|\mathbf{r}-x_0\hat{\mathbf{i}}-y^*\hat{\mathbf{j}}\right|^2}.$$

Here (x_0, y^*) is the position of the virtual source and $\mathbf{r} = x\hat{\mathbf{i}} + y\hat{\mathbf{j}}$ is the position vector of the target point. When $x \to x_0^+$ the depth-integrated flow vector above becomes orthogonal to $\hat{\mathbf{i}}$ (unit vector

directed to the open sea) for $y \neq y^*$. On the other hand, the total seaward flux associated with the depth-integrated flow vector above is unity because

$$\int_{-\infty}^{\infty} dy \frac{1}{\pi} \frac{\mathbf{r} - x_0\hat{\mathbf{i}} - y^*\hat{\mathbf{j}}}{|\mathbf{r} - x_0\hat{\mathbf{i}} - y^*\hat{\mathbf{j}}|^2} \cdot \hat{\mathbf{i}} = 1$$

(see Ref. [11], p. 94) for $x > x_0$. One can then reach the conclusion that the depth-integrated fluid velocity in the x direction (Hu) associated with a wave given by $\eta = \omega/(2gH)\mathrm{H}_0^{(2)}(\frac{\omega}{\sqrt{\mathrm{gH}}}|\mathbf{r} - \mathrm{x}_0\hat{\mathbf{i}} - \mathrm{y}^*\hat{\mathbf{j}}|)\exp(\mathrm{i}\omega\mathrm{t})$ satisfies

$$\lim_{x \to x_0^+} Hu(t, x, y) = \delta(y - y^*)\exp(i\omega t), \tag{9}$$

where $\delta(y - y^*)$ is a Dirac function. The continuity of Hu across the mouth of the rectangular bay requires

$$\tilde{s}(\omega, y^*) \approx \frac{igH}{\omega}\left[-B_0(\omega)\frac{\omega}{\sqrt{gH}}\sin\left(\frac{\omega}{\sqrt{gH}}x_0\right) + \sum_{n=1}^{\infty} B_n(\omega)\sqrt{\left(\frac{n\pi}{Y_0}\right)^2 - \frac{\omega^2}{gH}}\cos\left(\frac{n\pi}{Y_0}y^*\right)\right], \tag{10}$$

where function tanh with large argument has been approximated by 1. Now the waves inside and outside of the bay are a function of coefficients $B_0(\omega), B_1(\omega), \ldots, B_N$ as $\tilde{s}$ has been eliminated from (8) using (10). Let $\tilde{\eta}$ denote the temporal Fourier transform of η. The coefficients,$B_0(\omega), B_1(\omega), \ldots,$ will be chosen to minimize the penalty integral

$$\int_{-Y_0}^{Y_0} dy|\tilde{\eta}^{\mathrm{open}}(\omega, x_0^+, y) - \tilde{\eta}(\omega, x_0^-, y)|^2 \tag{11}$$

for each frequency. Using Gaussian quadrature, the penalty integral can be transformed into a finite summation

$$\sum_{m=1}^{M} w_m|\tilde{\eta}^{\mathrm{open}}(\omega, x_0^+, y_m) - \tilde{\eta}(\omega, x_0^-, y_m)|^2 \tag{12}$$

with $N + 1 < M$ where $N + 1$ is the number of unknowns. Here w_m's and y_m's are weights and nodes of the Gauss quadrature, respectively. The least-squares solution of the overdetermined system of equations below:

$$\sqrt{w_m}\tilde{\eta}(\omega, x_0^-, y_m, B_0, B_1, \ldots, B_N) = \sqrt{w_m}\tilde{\eta}^{\mathrm{open}}(\omega, x_0^+, y_m, B_0, B_1, \ldots, B_N) \tag{13}$$

for $m = 1, 2, \ldots, M$ leads to coefficients $B_0(\omega), B_1(\omega), \ldots, B_N(\omega)$ with $B_0(\omega)$ being the temporal Fourier transform of the run-up. In obtaining $\tilde{\eta}^{\mathrm{open}}(\omega, x_0, y)$ as a linear function of $B_0, B_1, \ldots, B_N$ the Hankel function with logarithmic singularity needs to be integrated with respect to y. In the vicinity of the singularity, we divide the Hankel function by a log and approximate this ratio by a polynomial. We then multiply this with the log function again and integrate it analytically. The solution obtained from the minimization of the penalty integral (12) is more accurate than all other approaches that will be presented in this article; therefore, hereafter we will refer to it as "exact."

In order to proceed to the inverse Fourier transform of $B_n(\omega)$ we resort to the fast Fourier transform. For this purpose the incident wave at the toe of the shelf is sampled at instants $0, T/P, 2T/P, \ldots, (P-1)T/P$ where P is an exact power of two. Here note that coefficients $B_N(\omega)$ are calculatef at those discrete frequencies equal or inferior to the Nyquist frequency ($P\pi/T$). For frequencies higher than the Nyquist frequency we use the reality condition, which states that for a real-valued incident wave the wave inside the bay remains real. A real incident wave means that

$$I_0\left(\omega = \frac{p2\pi}{T}\right) = \bar{I}_0\left(\omega = \frac{-p2\pi}{T}\right) = \bar{I}_0\left(\omega = \frac{-p2\pi}{T} + P\frac{2\pi}{T}\right), \quad p = 0, 1, 2, \ldots, P-1, \tag{14}$$

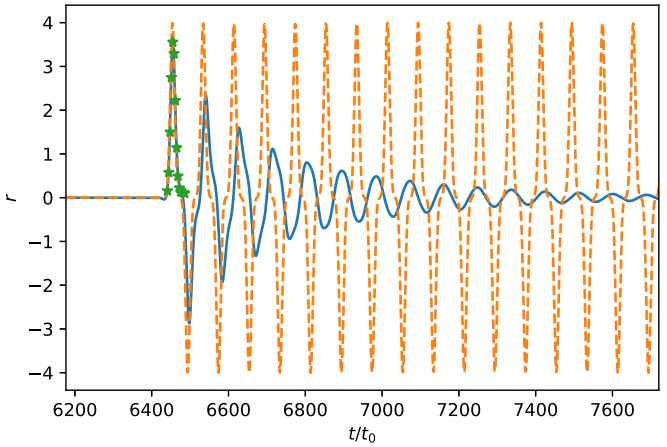

FIG. 3. Run-up generated by a Gaussian incident wave given by $\exp\{-[(x+\sqrt{gH_0})(t-T/2)/(0.4x_0)]^2\}$ entering a rectangular bay of aspect ratio $x_0/(2Y_0)=10$. The continuous curve is the "exact" solution of integral equation, dashed curve is $r^{(0)}(t)$ (undisturbed solution of Dirichlet problem), and the stars are $r^{(0)}(t)+r^{(1)}(t)$. The timescale t_0 is $Y_0/\sqrt{gH}$, and T is the duration of sampling. Maximum run-up associated with $r^{(0)}$ and $r^{(0)}+r^{(1)}$ is 4.0 and 3.6, respectively. The "exact" maximum is 3.52.

where the overbar denotes the complex conjugate. Here T is taken so large that all the waves within the bay, generated by the incident packet, die out because of the radiation to the open sea.

The run-up generated by a a Gaussian wave train entering a rectangular bay is displayed in Fig. 3, where maximum run-up obtained from the Dirichlet condition (dashed curve) exceeds that obtained from (7) by 13.6% (continuous curve).

III. WAVES IN AN INCLINED BAY OF PARABOLIC CROSS SECTION

Let us consider an inclined bay with a parabolic cross section whose bottom coordinates are given by

$$z=-\alpha x+y^2/y_0, \tag{15}$$

where $z=0$ is the undisturbed free surface. The half width of the bay at its entrance is then $Y_0=\sqrt{\alpha y_0 x_0}$. The relation between the uniform depth $H_{\max}$ of the open sea and the length of the bay is $H_{\max}=\alpha x_0$ (see Fig. 4).

Let us consider a progressive wave with an intermediate wavelength advancing in a converging bay of arbitrary shape. By intermediate wavelength is meant a length scale much shorter than the bay length but still much larger than the bay width. For such a wave the shape of the cross section of the bay does not vary much within one wavelength so that the transmitted power is preserved. The transmitted power is

$$S_0(x)g\rho\bar{\eta}(t,x)\bar{u}(t,x) \tag{16}$$

with $\bar{u}$ being proportional to $\bar{\eta}/\sqrt{\bar{H}(x)}$ for a progressive wave (see Ref. [11], p. 117). Here $S_0(x)$ is the undisturbed area of the cross section of the bay. Bars over the symbols denote the averaged values along the width of the bay. Due to the conservation of energy flux [given by (17)], the approximate form of the progressive wave inside a smooth bay of arbitrary shape is (see Ref. [23])

$$\bar{\eta}(t,x)\approx\int d\omega\frac{2\tilde{I}_0(\omega)\exp\left\{i\left[\omega t+\int_{x_0}^{x}k(\omega,x')\,dx'\right]\right\}}{\sqrt{S_0(x)/S_0(x_0)}[\bar{H}(x)/\bar{H}(x_0)]^{-1/4}}, \tag{17}$$

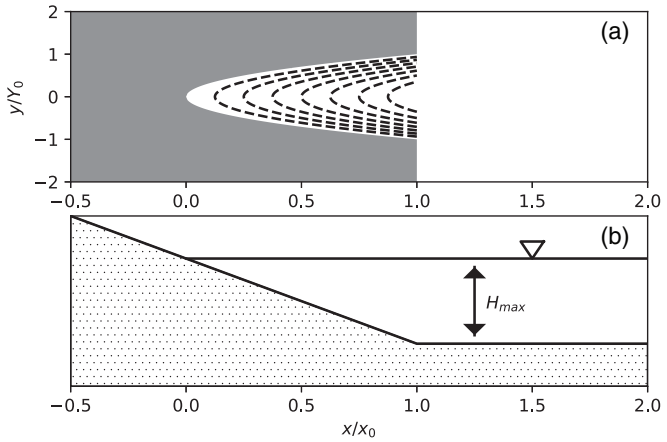

FIG. 4. (a) The inclined bay with a parabolic cross section seen from above. The broken curves are contours of equal depth given by $z_k = -k\,H_{\max}/8$ with $k = 1, 2, \ldots, 7$. Any point (x, y, z) at the bottom of the bay satisfies $z = -\alpha x + y^2/y_0$ with $H_{\max} = Y_0^2/y_0$. (b) The bay seen from the side depicting the plane, $y = 0$. The slope, α, is $H_{\max}/x_0$.

where $k(\omega, x)$ is $\omega/\sqrt{g\bar{H}(x)}$, and $\tilde{I}_0(\omega)$ is a Fourier transform with respect to time of the incident wave train at $x = x_0^+$. For an inclined bay with parabolic cross section, S_0 is proportional to $x^{3/2}$ and $\bar{H}$ to x. Taking these relations into account (17) is reduced to

$$\bar{\eta}(t, x) \approx \int d\omega \frac{2\tilde{I}_0(\omega) \exp\left\{i\left[\omega t + \int_{x_0}^{x} k(\omega, x')\, dx'\right]\right\}}{\sqrt{x/x_0}}. \tag{18}$$

Carrying out the integration with respect to x' and ω,

$$\bar{\eta}(t, x) \approx 2\sqrt{\frac{x_0}{x}}\,\eta_{\text{inc}}^{\text{open}}\left(t - \sqrt{\frac{6}{\alpha g}}(\sqrt{x_0} - \sqrt{x}), x_0^+\right) \tag{19}$$

is obtained. However (19) becomes exact when S_0 is proportional to $x^{3/2}$. Waves described by (19) are called nonreflecting because the phase of a wave inside the bay is simply a function of $t - \sqrt{6x/(\alpha g)}$, thus exclusively a progressive wave. They, therefore, do not reflect until they arrive the inland tip of the bay. The reflected wave by the inland tip of the bay has opposite polarity because the power transmitted to the tip is zero. When the incoming and the reflected waves of opposite signs are added in the vicinity of the inland tip (x being infinitesimally small), the difference between their phases becomes proportional to $\sqrt{x}$, thus the wave amplitude being finite, at any given instant t. It was already mentioned that the wave that is traveling in the offshore direction when reflected by the mouth of the bay has its polarity reversed because these waves do no affect the water level at $x = x_0$ due to the Dirichlet boundary condition. After two reflections the original polarity is recovered. A wave that progresses toward the mouth of the bay has undergone an odd number of reflections, while a wave approaching the inland tip of the bay has been exposed to an even number of reflections (0, 2, ...). Summing all these reflections the profile of the wave within the bay can be found as

$$\bar{\eta}(t, x) \approx \sum_{k=0}^{\infty} 2\sqrt{\frac{x_0}{x}}\left\{\eta_{\text{open}}^{\text{inc}}[t + \tau_0\sqrt{x/x_0} - (2k+1)\tau_0, x_0^+]\right.$$
$$\left. - \eta_{\text{open}}^{\text{inc}}[t - \tau_0\sqrt{x/x_0} - (2k+1)\tau_0, x_0^+]\right\}, \tag{20}$$

TABLE I. The maximum run-ups for various Gaussian incident waves given by $\exp[-(x+\sqrt{gH_0}t/L)^2]$ entering inclined bays of different aspect ratios. All bays have parabolic cross sections. The values within the parentheses in the columns of the table are run-ups obtained from the "exact" solution given by (43) and from the solution where the Dirichlet boundary condition has been imposed (21), respectively.

	$L = 20Y_0$	$L = 16Y_0$	$L = 12Y_0$	$L = 8Y_0$
$x_0 = 20Y_0$	(8.32,8.4)	(10.16,10.5)	(13.,14.)	(18.6,21)
$x_0 = 10Y_0$	(4.36,4.19)	(5.32,5.23)	(6.87,7.)	(9.53,10.5)
$x_0 = 5Y_0$	(2.54,2.37)	(2.94,2.73)	(3.6,3.49)	(5.16,5.23)

where τ_0 is one-way travel time along the bay $[\sqrt{6x_0/(\alpha g)}]$. The resulting run-up $r(t) = \eta(t, x = 0)$ according to Ref. [21] can be obtained using L'Hôpital's rule:

$$r(t) \approx \sum_{k=0}^{\infty} 4\tau_0 \left[\frac{\partial}{\partial t} \eta^{\text{inc}}_{\text{open}}(t - (2k+1)\tau_0, x_0^+) \right]. \tag{21}$$

Note that the run-up is proportional to the length of the bay because $\tau_0 = \sqrt{6x_0/(\alpha g)}$ is equal to $x_0/\sqrt{6Hg}$. For the case of the infinitely wide (independent of y) sloping beach of length x_0 connected to a sea of uniform depth the run-up is proportional to $\sqrt{x_0}$ if the wavelengths of the incident wave are much smaller than x_0 (see Ref. [23]). Thus converging bays generate a larger run-up than those of the infinite sloping beaches.

A consequence of the Dirichlet condition is the run-up being a periodical function of time even when the incident wave train is not. In the next section we will show that when the series in Eq. (21) is truncated to its few terms it produces more realistic run-ups because the artificial periodicity imposed by the Dirichlet condition is canceled. An incident N-wave in the open sea may have slopes of the same sign in its front and tail. If the distance between the regions of positive slopes is about $2\tau_0\sqrt{gH_{\max}}$, then the wave from these parts may interfere constructively to generate a larger run-up.

If the period of the incident wave in the open sea is much larger than the travel time (τ_0) of the waves along the bay, then the summation in Eq. (21) can be seen as a Riemann sum with integration step $2\tau_0$, and the run-up will be approximated by

$$r(t) \approx 2\int_{-\infty}^{t} dt\, \frac{\partial}{\partial t} \eta^{\text{inc}}_{\text{open}} = 2\eta^{\text{inc}}_{\text{open}}(t, x_0). \tag{22}$$

This was an expected result because with such long waves the displacement of the free surface at the tip and at the mouth of the bay must be almost equal. Note that this result is independent of any geometric characteristic (except the length) of the bay, reflecting the physical phenomenon of water slowly invading everywhere simultaneously, in a way reminiscent of the principle of communicating vessels (see Ref. [24]). Indeed, it will be shown in Table I that the normalized run-up for waves longer than the length of the bay is close to two as suggested by (22).

To show the difference of behavior of waves in reflecting and nonreflecting bays two longitudinally infinitely long inclined bays are considered, one with a parabolic cross section (nonreflecting) and the other with a rectangular cross section and constant width. The slope of the rectangular bay is $2\alpha/3$ so that both bays have the same laterally averaged depth for a given x. In the nonreflecting bay with a parabolic cross section, the wave train reflected by the inland tip is related to the initial incident wave through the relation [consider the second line of (20) for $k = 0$],

$$\bar{\eta}_{\text{ref}}(t, x) = -\sqrt{\frac{\tau^{-1}[t - \tau(x)]}{x}}\, \eta_{\text{inc}}(t = 0, x + \tau^{-1}[t - \tau(x)])\theta[t - \tau(x)], \tag{23}$$

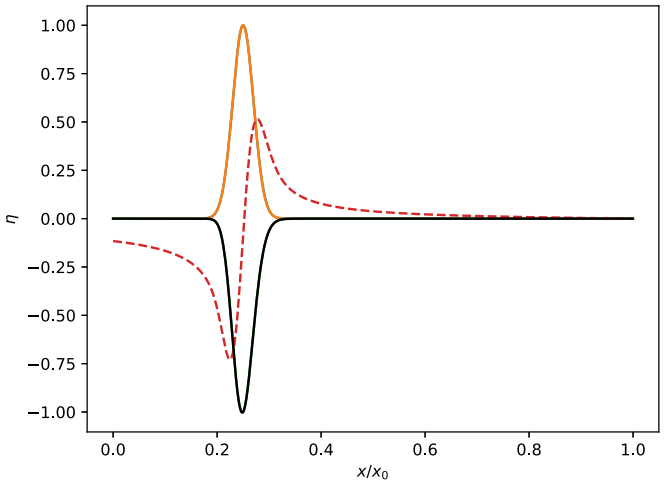

FIG. 5. The positive continuous curve is the initial profile of the incident wave given by $\exp[-\frac{1}{2}(\frac{x-x_1}{a})^2]$. The incident wave is progressing in an inclined bay with a parabolic cross section. The bottom of the bay is $z=-\alpha x+y^2/y_0$. The depression is the wave profile at instant $t=2\int_0^{x_1}\frac{dx}{\sqrt{2g\alpha x/3}}$ (the denominator in the integrand is the wave speed). The broken curve is the wave profile at instant t for the same incident wave progressing over a sloping bay with a rectangular cross section whose slope is $\frac{2}{3}\alpha$. In both geometries the averaged depths for a given x are equal. The values of parameters are $x_1=x_0/4$, $a=0.02x_0$ (x_0 is an arbitrary length scale). Note that for the case of a sloping bay with a rectangular cross section the incident wave starts to be reflected before reaching $x=0$.

where the function $\tau(x)$ is $\sqrt{6x/(g\alpha)}$. The step function θ in the above equation is due to the fact that reflection from the inland tip starts at $t=0$. On the other hand, in the case of an inclined rectangular bay, defining σ as $\sqrt{6x/(g\alpha)}$ a general solution of LSW averaged over the width of the bay becomes

$$\bar{\eta}(t,x)=\int_0^\infty d\omega\, J_0(\omega\sigma)[a(\omega)\cos(\omega t)+b(\omega)\sin(\omega t)/\omega] \tag{24}$$

according to Ref. [25]. Here J_0 is Bessel function of the zeroth order. Coefficients $a(\omega)$ and $b(\omega)$ can be obtained by proceeding to a Hankel transform of $\bar{\eta}(t=0,\sigma)$ and $\partial_t\bar{\eta}(t,\sigma)|_{t=0}$, respectively $[a(\omega)=\int_0^\infty d\sigma\sigma J_0(\omega\sigma)\bar{\eta}(t=0,\sigma)]$. The wave given by (24) can emulate a wave which initially progresses toward the coast if $\partial_t\bar{\eta}(t=0,x)|_{t=0}$ is equal to $\sqrt{gH(x)}\partial_x\bar{\eta}(t=0,x)$ according to Ref. [5], p. 84 (assuming the breadth of the wave train is much less than the distance to the inland extremity of the inclined bay). The snapshots of the wave generated by Eqs. (23) and (24) are displayed in Fig. 5. Although these two examples share the same initial conditions, a reflected wave in the case of a reflecting bay (inclined rectangular) reaches higher x coordinates than that of the nonreflecting bay because in the first case the wave starts to be reflected before reaching the inland tip of the bay.

To understand the mechanism of continuous reflection in reflecting bays one can consider an inclined bay with a rectangular cross section of constant width. A solution in such a geometry is $\eta=J_0(2\omega\sqrt{\frac{x}{g\alpha}})\exp(i\omega t)$. Here the Bessel function J_0 is a superposition of Hankel functions $[J_0=\frac{1}{2}(H_0^{(1)}+H_0^{(2)})]$. In the deeper parts of the bay, Hankel functions can be reduced to the first term of their asymptotic expansion, and therefore waves associated with them are progressive waves traveling in opposite directions $[H_0^{(1,2)}(z)\propto\exp(+-iz)/\sqrt{z}]$. Thus, with $\omega>0$, $\eta=H_0^{(1)}(2\omega\sqrt{\frac{x}{g\alpha}})\exp(i\omega t)$ is an incident wave within the bay. However, the Hankel function $H_0^{(1)}$ does not represent a progressive wave very close to the inland tip of the bay (for small values of x). The

reason it is not progressive is because the associated energy flux, denoted as J, is not equal to the following entity:

$$-\sqrt{gH(x)}\left[\tfrac{1}{2}\rho g\eta^2+\tfrac{1}{2}\rho H(x)v^2\right], \tag{25}$$

where the term in the brackets is the energy density. The minus sign is due to the fact that $H_0^{(1)}(2\omega\sqrt{\frac{x}{g\alpha}})\exp(i\omega t)$ is an incident wave. The energy flux associated with $H_0^{(1)}$ is a preserved quantity as energy density averaged over one cycle does not change with time. For small values of x the kinetic energy density becomes proportional to $1/x$ with $H_0^{(1)}(z)\approx\frac{2i}{\pi}\ln(z)$. This divergence near the coastline is at odds with the preservation of J, which becomes proportional to $1/\sqrt{x}$ according to (25). Therefore, this Hankel function does not represent a single progressive wave near the coastline. The only way for the energy density divergence with finite energy transmission is to have two progressive waves of different amplitudes propagating in opposite directions. In such a case it is possible for the transmitted power to be arbitrarily smaller than suggested by (25).

A. Comparison with a numerical experiment

In Ref. [26] a numerical experiment was carried out for a geometry where there is an inclined wall containing a concave semicylinder, reminiscent of an inclined bay of a parabolic cross section. We compared their maximum run-ups with ours where an incident soliton of amplitude 0.035 m hits a parabolic bay of length $x_0=H_{\max}/\tan(\theta)+R$ and width $2R$ at its mouth. Here $H_{\max}=0.35$ m is the maximum depth of the parabolic bay [see Fig. 4(b)], $R=1.2$ m is the radius of the cylinder, and θ is the inclination angle. We used the first term of the summation in Eq. (21) (we neglect multiple reflections) and also modified the factor 4 to 2. The reason we modified this factor is related to the aspect ratio of their bay with a greater width than length, violating the assumption that the waves reflecting from the outside lateral walls at the entrance of the bay are equal to the amplitude of the incident wave. Also, to adapt to the geometry of Ref. [26] we changed the travel time τ used in Eq. (21) to $\int_0^{x_0}\frac{dx}{\sqrt{gH(x)}}$ where $H(x)$ is the laterally averaged depth according to the setting given in Ref. [26].

For inclination angles $30^\circ, 45^\circ$, and 60° the maximum run-ups are 0.113 m, 0.088 m, and 0.072 m, respectively, according to a modified (21). The run-up 0.113 m overshoots the computational result of Ref. [26] by about 5%. This overshooting was expected because in Ref. [26] the sloping side banks of the bay are completely submerged near the mouth of the bay, making the trapping of waves inside the bay less effective. For a steeper inclination, our approach underestimates the run-up (20% underestimation for $\theta=60^\circ$) mainly because for larger inclinations the bay is shorter and the assumption that the exponentially decaying part of (7) (the summation) may still be somewhat significant at the inland tip of the bay. In general, the three-dimensional nature of the flow becomes more prominent for greater inclinations, therefore the shallow water approach performs poorly.

IV. EXACT BOUNDARY CONDITIONS AT THE ENTRANCE OF THE BAY

In this section we will match η and $H(x,y)\partial_x\eta$ across the mouth of the bay. For this purpose two-dimensional solutions of LSW equations must be found inside the bay. It was already mentioned that the solutions that depend strongly on y coordinates are confined to the vicinity of the mouth of the bay where the relative depth variation in the x direction is small. Therefore the bay will be approximated by a channel of uniform cross section (basically a noninclining channel of parabolic cross section) in this region. The two-dimensional LSW equation is

$$\frac{\partial^2}{\partial t^2}\eta-g\left\{\frac{\partial}{\partial x}\left[H(y)\frac{\partial}{\partial x}\eta\right]+\frac{\partial}{\partial y}\left[H(y)\frac{\partial}{\partial y}\eta\right]\right\}=0, \tag{26}$$

where the depth $H(y)$ is $H_{\max}[1-(y/Y_0)^2]$ in the vicinity of the mouth. For depth, independent of x the solution of the LSW equation is in the form

$$\eta_\omega = \exp[\kappa(\omega)x] f_\kappa(y) \exp(i\omega t), \tag{27}$$

where $\kappa(\omega)$ multiplied by i is the wave number within the parabolic channel. Defining nondimensional y' as y/Y_0, the function f_κ must satisfy the ordinary differential equation

$$-\frac{\omega^2 Y_0^2}{g\alpha x_0} f_\kappa(y') - \kappa^2 Y_0^2 (1-y'^2) f_\kappa(y') - \frac{d}{dy'}\left[(1-y'^2)\frac{d}{dy'} f_\kappa(y')\right] = 0. \tag{28}$$

This ordinary differential equation has two singular points $y' = \pm 1$. Given ω (which we will take to be equal to the frequency of the incident wave), if the parameter κ takes some discrete values, $\kappa_0(\omega), \kappa_1(\omega), \ldots$, then the solution will become regular at both singular points (our aim is to determine those particular κ values). In the case of such regularity the depth-integrated fluid velocity in the *y direction* tends to zero at the sides of the channel ($y' \to \pm 1$). The situation is very similar to the case of rectangular channel where the n in Eq. (7) needed to be an integer in order to satisfy the no-flux condition at the sides of channel.

Equation (28) in terms of the wave vector of the incident wave ($k_{\text{inc}}^{\text{open}} = \omega/\sqrt{g\alpha x_0}$) becomes

$$\kappa^2 Y_0^2 (1-y'^2) f_\kappa(y') = -\left(k_{\text{inc}}^{\text{open}} Y_0\right)^2 f_\kappa(y') - \frac{d}{dy'}\left[(1-y'^2)\frac{d}{dy'} f_\kappa(y')\right]. \tag{29}$$

Only solutions that are even functions of y' will be taken into account because of the symmetry of the incident wave. Note that the eigenfunctions of the differential operator, $\frac{d}{dy'}[(1-y'^2)\frac{d}{dy'}]$, in the equation above are Legendre polynomials

$$P_l(y')$$

with eigenvalues

$$-l(l+1) \quad \text{with} \quad l = 0, 1, 2, \ldots .$$

We can now expand $f_\kappa(y')$ in terms of these eigenfunctions:

$$f_\kappa(y') = \sum_{l=0}^{\infty} A_{2l}^{(\kappa)} \sqrt{2l+0.5} P_{2l}(y'). \tag{30}$$

Inserting the series above into (29) and using relations

$$y' P_l(y') = \frac{1}{2l+1}[(l+1)P_{l+1}(y') - lP_{l-1}(y')] \quad \text{and} \quad \mathrm{y'P_0(y') = P_1(y')}$$
$$\frac{d}{dy'}\left[(1-y'^2)\frac{d}{dy'}\right] P_l(y') = -l(l+1)P_l(y'), \tag{31}$$

the term, y'^2, and the derivatives of P_{2l} can be eliminated from the series. The left-hand side of (29) is then reduced to a series of Legendre polynomials with constant coefficients involving $A_{2l}^{(\kappa)}$'s. Equating the coefficients of $P_{2l}(y')$ at both sides of (29), a recurrence relation between $A_{l-2}^{(\kappa)}$, $A_l^{(\kappa)}$, and $A_{l+2}^{(\kappa)}$ is found. For the particular case of $l = 0$, $A_2^{(\kappa)}$ is proportional to $A_0^{(\kappa)}$ with

$$A_2^{(\kappa)}/A_0^{(\kappa)} = -\tfrac{1}{2}\left[\left(k_{\text{inc}}^{\text{open}} Y_0\right)^2 + (\kappa Y_0)^2\right].$$

For some discrete values of the eigenvalue, $(\kappa Y_0)^2$, coefficients $A_{2l}^{(\kappa)}$ obtained from the recurrence relation tend to zero for $l \to \infty$. The value of $A_0^{(\kappa)}$ is arbitrary. For the energy-transmitting mode A_0^{κ} is taken 1 so the associated function, $f_\kappa(y')$, will be approximately 1 in the low-frequency limit. In the Appendix an alternative method that is easier to implement in Python using a linear algebra package is presented. Eigenvalues $[(\kappa Y_0)^2]$ computed by the linear algebra package will be referred

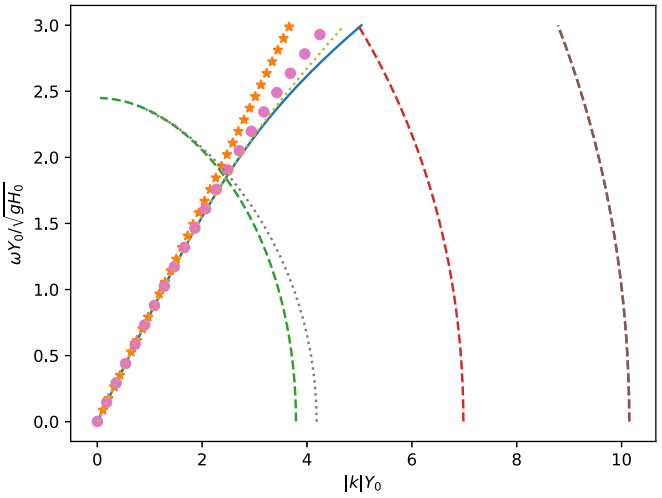

FIG. 6. The continuous and the broken curves are the dispersion relations for an infinite channel with a parabolic cross section. Broken curves indicate a purely imaginary wave vector. The waves associated with such wave vectors decay exponentially in the $-x$ direction because they are proportional to $\exp(|k|x)$. Continuous and broken curves were obtained using the routine `eigh` (see the Appendix). The equation of the bottom of the channel is $z = -H_{\max}(1 - y^2/Y_0^2)$ where H is its maximum depth and Y_0 is its half width. The stars are the dispersion relation given by $\omega = \sqrt{g2H_{\max}/3}\,|k|$ where $2H/3$ is the average depth of the parabolic channel. The circles are the dispersion relation obtained using Eq. (2.51) from Ref. [17]. The dots (two branches) are the dispersion relation obtained from (40).

to as "exact" eigenvalues because they are more accurate than various approximations that will be made later. An ordinary differential equation given by (29) is similar to the differential equation for an angular prolate spheroidal wave function [see Eq. (21.6.1) in Ref. [22]]. In the context of the angular spheroidal differential equation the term denoted in Eq. (29) as $(k_{\text{inc}}^{\text{open}}Y_0)$ is the quantity to be determined. This quantity in that context is called the separation constant. Our aim in solving the LSW equation was to determine $(\kappa Y_0)^2$ as a function of the frequency of the incident wave. Because of this discrepancy the libraries for spheroidal functions were not used.

In Fig. 6 the inverse of the relation between κ and ω is displayed (see the Appendix for the relation). In that figure one can observe that given a nondimensional frequency $(\omega Y_0/\sqrt{g_0 H_0})$ less than $\sqrt{6}$ there is only one mode with negative $(\kappa Y_0)^2$ (the continuous curve in Fig. 6). Negative $(\kappa Y_0)^2$ corresponds to a real wave vector inside the bay, thus transmitting energy in the x direction. Our hypothesis was that the modes depending strongly on y coordinate are confined to the vicinity of the mouth of the bay. If there were two modes with a real wave vector, then the hypothesis would be violated as the second mode is roughly proportional to $P_2(y')$, and thus *not* independent of y. Our analysis will be valid for incident waves with the dominant frequency satisfying $\omega Y_0/\sqrt{gH_{\max}} < \sqrt{6}$. The reason why the nondimensional cutoff frequency is exactly $\sqrt{6}$ will be clarified below. A purely complex wave vector $[(\kappa Y_0)^2 > 0]$ cannot transmit power because u ad η will be off phase by $\pi/2$.

In an infinite rectangular channel of the equivalent averaged depth $(2H_{\max}/3)$, there will be only one energy-transmitting mode if $\omega Y_0/\sqrt{gH_{\max}}$ is less than $2.56 \approx \sqrt{2/3}\,\pi$. Note that the eigenvalues of the differential operator at the right-hand side of (29) acting on even eigenfunctions are

$$-\left(k_{\text{inc}}^{\text{open}}Y_0\right)^2 + 2l(2l+1) \quad \text{with} \quad l = 0, 1, 2, \ldots. \tag{32}$$

If the nondimensional wave number $(k_{\text{inc}}^{\text{open}}Y_0) < \sqrt{6}$, then only the first mode (associated with $l = 0$) can propagate, and higher modes cannot.

The eigenvalues, $(\kappa Y_0)^2$, will be numbered in ascending order:

$$(\kappa_0 Y_0)^2 < 0 < (\kappa_1 Y_0)^2 < (\kappa_2 Y_0)^2 < \cdots . \tag{33}$$

Only mode 0 is then capable of transmitting energy. The dispersive nature of the relation between ω and $|\kappa_0 Y_0|$ becomes apparent for $|\kappa_0 Y_0| > 2$ where clearly

$$\frac{d^2}{dk^2}\omega < 0$$

with $k = i|\kappa_0|$. According to Fig. 6 the approximation made in Ref. [17] for the dispersion relation is far better than that obtained from laterally averaging depth ($\omega = \sqrt{g\bar{H}}k$). However, the dispersion relation in Ref. [17] slightly overestimates the frequencies (compare circles with the continuous curve in Fig. 6). This *small* overestimation can be explained on the basis of a variational formulation of the eigenvalue problem.

In the above calculation, our aim was to calculate different κ values given ω, the frequency of the incident wave. Alternatively, we can calculate ω, given κ. For a given real wave vector $k = |\kappa_0|$ inside the parabolic infinite channel, the square of the associated frequency, $\omega^2 Y_0^2/(gH_0)$, can be found minimizing the following Rayleigh quotient:

$$\frac{\int_{-1}^{1} dy\left\{|\kappa_0|^2 Y_0^2(1-y^2)f^2(y) + (1-y^2)\left[\frac{d}{dy}f(y)\right]^2\right\}}{\int_{-1}^{1} dy\, f^2(y)} \tag{34}$$

with respect to f. The variation of Rayleigh quotient [see (34)] around the minimizing function, f_{κ_0}, leads to

$$\frac{-\int_{-1}^{1}\left\{|\kappa_0|^2 Y_0^2(1-y^2)f_{\kappa_0}^2(y) + (1-y^2)\left[\frac{d}{dy}f_{\kappa_0}(y)\right]^2\right\}dy}{\left[\int_{-1}^{1} dy f_{\kappa_0}^2(y)\right]^2} \times \left[\int_{-1}^{1} dy f(y)\delta f(y)\right]$$
$$+\frac{\left\{|\kappa_0|^2 Y_0^2(1-y^2)f_{\kappa_0}(y) - \frac{d}{dy}\left[(1-y^2)\frac{d}{dy}f_{\kappa_0}(y)\right]\right\}\delta f(y)}{\left[\int_{-1}^{1} dy f_{\kappa_0}^2(y)\right]}, \tag{35}$$

where the second term in the numerator of the last line has been obtained by integration by parts. No contribution comes from the bounds of the integral because f_{κ_0} is bounded at $y = \pm 1$. Noticing that f_{κ_0} minimizes the Rayleigh quotient the first line of (35) is equal to $-\omega_0^2(gH_0)^{-1}[\int_{-1}^{1} dy f_{\kappa_0}^2(y)]^{-1}$. Accordingly the variation becomes

$$\frac{1}{\int_{-1}^{1} dy f_{\kappa_0}^2(y)}\int_{-1}^{1} dy\delta f(y)\left\{-\frac{\omega_0^2 Y_0^2}{gH_0}f_{\kappa_0}(y) + |\kappa_0|^2 Y_0^2(1-y^2)f_{\kappa_0}(y) - \frac{d}{dy}\left[(1-y^2)\frac{d}{dy}f_{\kappa_0}(y)\right]\right\}. \tag{36}$$

The variation must be zero for all variation δf since f_{κ_0} is a minimizing function. Therefore the minimizing function satisfies the ordinary differential equation given in Eq. (28). In Ref. [17] the function f_{κ_0} was approximated by a polynomial of degree two. That is the reason for the *small* overestimation (see circles in Fig. 6). When variation of η along the y axis is ignored ($f_{\kappa_0} =$ constant) the associated frequency is even higher (see the stars in Fig. 6). As mentioned earlier the strong dependence of the decaying modes on y coordinates can be observed in Fig. 7.

Here we are looking at the propagating modes of an infinite channel with a parabolic cross section. In this context, there is no open sea, and there is no incident wave. However, we can still parametrize the frequencies in terms of $\omega = \sqrt{gH_{\max}}k_{\text{inc}}^{\text{open}}$. For a given ω defined this way,

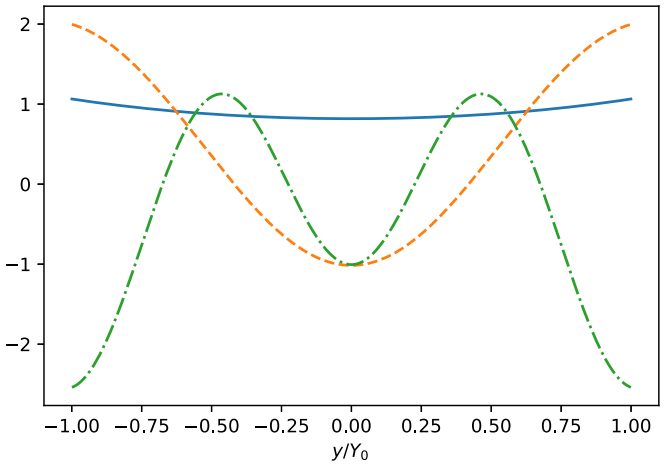

FIG. 7. The continuous curve represents the eigenfunction, $f_0(y,\omega)$, for $\omega Y_0/\sqrt{g\alpha x_0}=1$. See Eq. (30) for the definition of f_{κ_0}. The dashed and the dash-dotted curves are, respectively, f_{κ_1} and f_{κ_2}. The function f_{κ_0} is associated with the oscillatory solution in the x direction. Note that $f_{\kappa_0}(y)$ is almost constant.

the corresponding $\kappa^2 Y_0^2$ can be found minimizing the following Rayleigh quotient:

$$\frac{\int_{-1}^{1} dy\Big\{-\big(k_{\rm inc}^{\rm open}Y_0\big)^2 f^2(y)+(1-y^2)\big[\frac{d}{dy}f(y)\big]^2\Big\}}{\int_{-1}^{1} dy\,(1-y^2)f^2(y)}. \tag{37}$$

If we truncate (30) to the second order to produce the trial function $f(y)=A_0\sqrt{1/2}+A_2\sqrt{5/2}P_2(y)$, then the Rayleigh quotient becomes

$$\frac{(A_0,A_2)\begin{pmatrix}-(k_{\rm inc}^{\rm open}Y_0)^2 & 0\\ 0 & -(k_{\rm inc}^{\rm open}Y_0)^2+6\end{pmatrix}\begin{pmatrix}A_0\\A_2\end{pmatrix}}{(A_0,A_2)\begin{pmatrix}0.666 & -0.298\\ -0.298 & 0.476\end{pmatrix}\begin{pmatrix}A_0\\A_2\end{pmatrix}}. \tag{38}$$

The ratio above needs to be minimized with respect A_0 and A_2. At the minimizing (A_0,A_2) the gradient of the denominator and numerator of the Rayleigh quotient must be parallel with the constant proportionality between the gradients being $(\kappa Y_0)^2$. There is a no trivial (A_0,A_2) that makes these gradients parallel if the determinant of the following matrix vanishes:

$$\mathrm{Det}\begin{pmatrix}\Big[-\big(k_{\rm inc}^{\rm open}\big)^2-0.6666\kappa^2\Big]Y_0^2 & 0.2981(\kappa Y_0)^2\\ 0.2981(\kappa Y_0)^2 & \Big[-\big(k_{\rm inc}^{\rm open}\big)^2-0.4762\kappa^2\Big]Y_0^2+6\end{pmatrix}=0. \tag{39}$$

Solving the equation above, κ is obtained as a function of $\omega'=\omega Y_0/\sqrt{gH_0}$ as

$$|\kappa_n|Y_0=\begin{cases}\Big|\sqrt{\frac{4-1.141286\omega'^2-\sqrt{(-4+1.141286\omega'^2)^2-0.91428(\omega'^4-6\omega'^2)}}{0.45714}}\Big| & \text{if}\quad n=0\\ \Big|\sqrt{\frac{4-1.141286\omega'^2+\sqrt{(-4+1.141286\omega'^2)^2-0.91428(\omega'^4-6\omega'^2)}}{0.45714}}\Big| & \text{if}\quad n=1\end{cases}, \tag{40}$$

where $n=0$ corresponds to a purely complex κ, and it is, therefore, the energy-transmitting mode. The other is the decaying mode. Two branches of the dispersion obtained from (40) are displayed as dots in Fig. 6. The lower branch ($\omega=\omega(|\kappa_0|)$) obtained from (40) is more accurate than that given by Eq. (2.51) of Ref. [17] (compare the dotted curve and circles in Fig. 6); however, the difference between these two approximations becomes apparent only for frequencies larger than $\sqrt{6}\sqrt{gH_0}/Y_0$.

This range of frequencies is beyond the scope of the present work as the decaying modes will cease to be decaying for this range.

There are two waves associated with purely imaginary κ_0 (power-transmitting modes). One of these waves travels in the offshore direction and the other in the opposite direction. The full solution in the vicinity of the mouth (inside the bay) can be written as

$$\eta_\omega(t,x',y') = \exp(i\omega t)\Bigg\{[B_0^+\exp(i|\kappa_0|x) + B_0^-\exp(-i|\kappa_0|x)]f_{\kappa_0}(y') + \sum_{n=1}^{M-1} B_n \exp[|\kappa_n|(x-x_0)]f_{\kappa_n}(y')\Bigg\}. \tag{41}$$

The solution above can be extended to the whole of the inclined bay [21] using the fact that the phase difference, at a given instant, between two points separated by dx is $\pm|\kappa_0|\sqrt{x_0/x}\,dx$. Here the sign depends on the direction of travel of the wave. Integrating the argument of the exponential functions in the square brackets [Eq. (41)] from x_0 to x and multiplying the traveling wave by an appropriate factor to ensure conservation of energy flux [see (18)] η is found to be

$$\eta_\omega(t,x,y') = \exp(i\omega t)\Bigg\{\sqrt{\frac{x_0}{x}}\Big[B_0^+\exp(2i|\kappa_0|\sqrt{x_0x}\,) + B_0^-\exp(-2i|\kappa_0|\sqrt{x_0x}\,)\Big]f_{\kappa_0}(y') + \sum_{n=1}^{N} B_n\exp[|\kappa_n|(x-x_0)]f_{\kappa_n}(y')\Bigg\}. \tag{42}$$

Again the boundary condition at the inland tip of the bay requires that $B_0^+ = -B_0^-$. The decaying waves never reach $x=0$ because $|\kappa_n| \gg 1/x_0$ for $n = 1, 2, \ldots, N$. Taking into account the boundary condition at the tip (42) is reduced to

$$\eta_\omega(t,x,y') = \exp(i\omega t)\Bigg\{B_0^* j_0(2|\kappa_0|\sqrt{x_0x})f_{\kappa_0}(y') + \sum_{n=1}^{N} B_n\exp[|\kappa_n|(x-x_0)]f_{\kappa_n}(y')\Bigg\}, \tag{43}$$

where the spherical Bessel function $j_0(z)$ is $\sin(z)/z = \sqrt{\frac{\pi}{2z}}J_{1/2}(z)$. Here $J_{1/2}$ is the Bessel function of fractional order. The right-hand side of (43) is not a rigorous solution of laterally averaged LSW equations away from the mouth unless one makes the nondispersive approximations $|\kappa_0| \approx \omega/\sqrt{g\frac{2}{3}H_0}$ (see the stars and continuous curve in Fig. 6), but it is good enough for the practical purposes. Coefficients $B_0^*(\omega), B_1(\omega), B_2(\omega), \ldots, B_N(\omega)$ will be found from minimizing the penalty integral given by (11). However, the relation which relates the source strengths to these coefficients given by (10) needs to be modified because the depth is discontinuous at the mouth of the bay and the bay cross section is no longer rectangular. It becomes

$$\tilde{s}(\omega,y)\exp(i\omega t) = -H[1-(y/Y_0)^2]\frac{g}{i\omega}\frac{\partial}{\partial x}\eta_\omega(t,x,y)|_{x=x_0^-}, \tag{44}$$

where η_ω is given by the series in Eq. (43). For the run-up the only relevant coefficient is $B_0^*(\omega)$, and for $x=0$ the spherical Bessel function in Eq. (43) takes the value of one. Then the Fourier transform of the run-up, $\tilde{r}(\omega)$, is simply $B_0^*(\omega)A_0$ with A_0 being equal to one. In Fig. 8 the amplitude of run-up $r_\omega(t)$ is displayed as a function of the incident wave frequency (the amplitude of the incident wave is normalized to unity). Sharps peaks in that figure indicate that the poles of $\tilde{r}(\omega) = r_\omega(t)\exp(-i\omega t)$ in the complex ω plane are close to the real axis. The closeness of these poles to the real ω axis will be responsible of the effective trapping of energy of the wave inside the bay. The general trend in Fig. 8 is that $\tilde{r}(\omega) \propto \omega^1$. This is in agreement with the predictions of (21) where for a given frequency and depth the run-up was proportional to the length of the bay. As the ratio between the bay length and

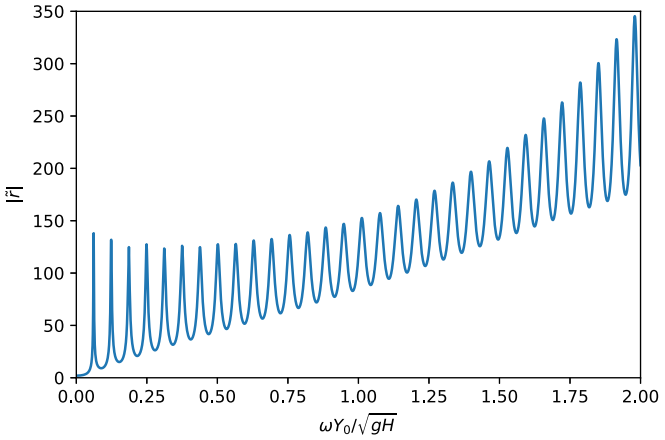

FIG. 8. Absolute value of Fourier transform of a run-up divided by that of the incident wave is displayed as a function of the nondimensional frequency, $\omega Y_0/\sqrt{gH}$. The length of the inclined parabolic channel is $x_0 = 10Y_0$ (Y_0 is half width at the mouth of the bay).

the wavelength increases, the run-up increases. On an infinitely wide, linearly sloping beach the run-up is proportional to $\omega^{1/2} I_0$ where I_0 is the amplitude of the incident wave at a distance L from the coast (see Ref. [23]). In the case of a converging bay the amplification of short waves is more effective because of the focusing of the energy towards the inland tip of the bay.

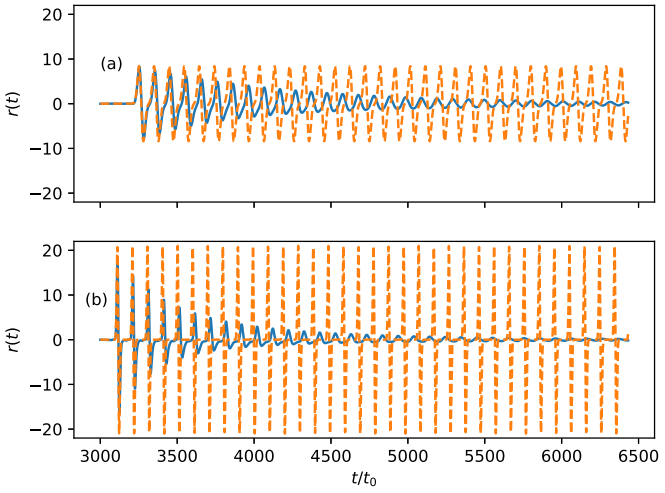

FIG. 9. Continuous curves are an "exact" run-up for an incident Gaussian waves calculated using (43). In (a) the incident wave in the open sea is $\exp\{-[x + \sqrt{gH_0}(t - T/2) - x_0]^2 x_0^{-2}\}$, and in (b) the narrower Gaussian is given by $\exp\{-[x + \sqrt{gH_0}(t - T/2) - x_0]^2 (0.4x_0)^{-2}\}$. The ratio $x_0/(2Y_0)$ is 10 for both cases. Here x_0 is the length of the bay, and $2Y_0 = 2\sqrt{\alpha x_0 y_0}$ is the width of the mouth of the bay [see (15) for the geometry of the bay]. The timescale t_0 is given by $Y_0/\sqrt{gH_0}$. The broken curves are the run-up associated with the Dirichlet problem $\eta(t, x_0^-) = 2\eta_{\text{inc}}^{\text{open}}(t, x_0^+)$ [see (21)]. Parameter T is the duration of the sampling of the incident wave. The solution associated with the Dirichlet boundary condition overestimates the maximum run-up by 1% in (a) and 12% in (b). The solutions associated with the Dirichlet boundary conditions are not damped. Note that two-way travel time along this bay are $97.98\, t_0 = 2\sqrt{6}\, x_0/\sqrt{gH_0}$.

The next step is to calculate the run-up for incident wave packets. In Fig. 9 two Gaussian incident wave packets of different widths

$$\eta_{\rm inc}^{\rm open(a,b)} = \exp\left[-(x+\sqrt{gH}(t-T/2)-x_0)^2 L_{(a,b)}^{-2}\right] \tag{45}$$

are considered. Here $L_{(a,b)}$ is x_0 in Fig. 9(a) and $0.4x_0$ in Fig. 9(b). Parameter T is the duration of the sampling. The continuous curves are associated with the solution obtained from (13) where $r(t)$ is the inverse Fourier transform of $\tilde{r} = B_0^*(\omega)$. The broken curves are run-ups from (21) (the Dirichlet boundary condition). The solution associated with the Dirichlet boundary condition overestimates the maximum run-up by 1% in Fig. 9(a) and 12 % in Fig. 9(b). In the introduction it was mentioned that the Dirichlet boundary condition is an accurate approximation of real boundary conditions for $\omega \ll \sqrt{gH_0}/Y_0$. That is why the predictions of (21) overestimate the maximum run-up by a higher margin in Fig. 9(b) where shorter wavelengths are involved. According to the approximate power law $\tilde{r}(\omega) \propto \omega^1$ one would expect the ratio between maximum run-ups in Figs. 9(a) and 9(b) to be 2.5 (the ratio of the$L$ values). It turns out the actual value of this ratio is 2.2. The failure of the relation, $r \propto \omega$, is due to the fact that the short incident waves cannot *capture* the general linear trend in Fig. 8. With increasing frequencies the poles of $\tilde{r}(\omega)$ move away from the real ω axis making the peaks at the right side of Fig. 8 broader. The rapid decay of oscillations in Fig. 9(b) is due to the fact that a narrower Gaussian excites modes with shorter wavelengths. The complex frequencies of homogeneous solutions of LSW in the bay are the poles of $\tilde{r}(\omega)$ in the complex ω plane. The homogeneous solutions with shorter wavelengths are associated with poles that are related to peaks at the right side of Fig. 8. Therefore they decay quickly transmitting their energy to the open sea.

V. PERTURBATION OF THE DIRICHLET BOUNDARY CONDITION

The Dirichlet boundary condition condition $[\eta(t,x_0^-) = 2\eta_{\rm inc}^{\rm open}(t,x_0^+)]$ leads to solutions that tend to overestimate the maximum run-up because the real sea level disturbance at $x = x_0^+$ is often less than $2\eta_{\rm inc}^{\rm open}(t,x_0^+)$. This is due to partial penetration of the incident wave into the bay. However, there are exceptions. If the characteristic wavelength of the incident wave packet is much longer than the length of the bay, situations may arise whereby the forward tail of the wave packet may reflect from the tip and the mouth of the bay multiple times before the maximum run-up occurs. These reverberations may cause constructive interference just outside the mouth, making the free surface disturbance *larger* than $2\eta_{\rm inc}^{\rm open}(t,x_0^+)$. Inspection of Table I reveals that the Dirichlet boundary condition indeed overestimates the maximum run-up when x_0 is larger than the wavelength.

A perturbative approach will be adopted where only one-dimensional solutions of the wave equation inside the bay will be required. The Dirichlet boundary condition is not "exact" because it violates the continuity of the depth-integrated x velocity across the mouth of the bay. When a scattered field into the open sea (the part of the wave field due to the presence of the bay) is ignored, the depth-integrated velocity is zero at $x = x_0^+$, but the sea level disturbance, $2\eta_{\rm inc}^{\rm open}(t,x_0^+)$, will trigger a wave progressing toward the inland tip of the bay. The simple relation between u and η for a wave progressing in the $-x$ direction is $u = -\sqrt{g/\bar{H}(x)}\,\eta$ where $\bar{H}(x)$ is the laterally averaged depth. Therefore the undisturbed Dirichlet condition imposes the following depth-integrated velocity at $x = x_0^-$:

$$H(x_0^-,y)u^{(0)}(t,x_0^-) = -H(x_0^-,y)\sqrt{g/\bar{H}(x_0^-)}\left[2\eta_{\rm inc}^{\rm open}(t,x_0^+)\right]. \tag{46}$$

Hereafter all quantities relating to the undisturbed Dirichlet condition will be referred to with the superscript (0). A distribution of virtual sources

$$s^{(1)}(t,y) = u^{(0)}(t,x_0^-)H(x_0,y) \tag{47}$$

placed at the entrance of the bay will ensure the continuity of depth-integrated velocity. The superscript (1) was used because sources $s^{(1)}$ will generate a scattered field $\eta_{\rm open}^{(1)}(t,x,y)$ in the open sea that will disturb the boundary condition $\eta(t,x_0^-) = 2\eta_{\rm inc}^{\rm open}(t,x_0^+)$. Evidently $\eta_{\rm open}^{(1)}(t,x,y)$ will be

a two-dimensional field depending strongly on the y coordinate. It will be shown that $\eta^{(1)}_{\text{open}}(t,x,y)$ is of order of $(\omega Y_0/\sqrt{gH})\eta^{\text{inc}}_{\text{open}}(t,x_0^+)$ within the relevant time range (before the full resonant regime sets in). In principle $\eta^{(1)}(t,x,y)$ must be continuous across the entrance of the bay, but because $\eta^{(1)}_{\text{open}}(t,x,y) \ll \eta^{\text{inc}}_{\text{open}}(t,x,y)$ this condition can be replaced by a less stringent one,

$$\eta^{(1)}(t,x_0^-) = \bar{\eta}^{(1)}_{\text{open}}(t,x_0^+) = \frac{1}{2Y_0}\int_{-Y_0}^{Y_0} dy\, \eta^{(1)}_{\text{open}}(t,x_0^+,y). \tag{48}$$

This simplification renders the problem one-dimensional within the inclined bay. The solution of the Dirichlet problem is identical to (20) for $k=0$:

$$\eta^{(1)}(t,x) = \sqrt{\frac{x_0}{x}}\left[\bar{\eta}^{(1)}\left(t - \frac{\sqrt{6x_0}(\sqrt{x_0}-\sqrt{x})}{\sqrt{gH}}, x_0^+\right)\right.$$
$$\left. - \bar{\eta}^{(1)}\left(t - \frac{\sqrt{6x_0}(\sqrt{x_0}+\sqrt{x})}{\sqrt{gH}}, x_0^+\right)\right] \quad \text{for} \quad 0 < \mathrm{x} < \mathrm{x}_0, \tag{49}$$

where the second line of the equation represents the wave reflected by the inland tip of the bay. Note that any function of $t \pm \sqrt{6x/(g\alpha)}$ is a solution of the laterally averaged LSW equation. Equation (49) will be valid as long as the waves reflected by the inland tip do not reach the entrance of the bay because the relation given by (46) holds only for waves progressing in the $-x$ direction.

The free surface perturbation $\eta^{(1)}(t,x)$ generates its own flow $u^{(1)}$ that will perturb the flux continuity at $x = x_0$. The same procedure needs to be repeated with $s^{(2)}$. The full iterative solution can be written as

$$s(t,y) = s^{(1)}(t,y) + s^{(2)}(t,y) + \cdots,$$
$$\eta(t,x) = \eta^{(0)}(t,x) + \eta^{(1)}(t,x) + \eta^{(2)}(t,x) + \cdots. \tag{50}$$

It will be shown that the series above converges rapidly if the relative variation of the incident wave within the timescale $t_0 = Y_0/\sqrt{gH_{\max}}$ is small. This will be the case if the characteristic wavelength of the incident wave is much larger than the width of the bay. The contribution from $\eta^{(i)}(t,x)$ to the run-up will be

$$r^{(i)}(t) = 4x_0\sqrt{\frac{6}{gH}}\frac{\partial}{\partial t}\eta^{(i)}\left(\sqrt{gH_{\max}}\left[t - x_0\sqrt{\frac{6}{Hg}}\right], x_0^-\right) \tag{51}$$

according to (21).

We will now show how explicitly $\eta^{(i)}(t,x_0^+)$ can be written as a function of $s^{(i)}(t',y)$ for $t > t'$. Let $g_r(t,x,y,t',x',y')$ be the retarded free surface response to a sudden fluid incursion of the *unit* volume into two-dimensional infinite sea at instant t' and at a position (x',y'). The function g_r will then satisfy the inhomogeneous equation,

$$\left[\frac{\partial^2}{\partial t^2} - gH\left(\frac{\partial^2}{\partial x^2} + \frac{\partial^2}{\partial y^2}\right)\right]g_r = \delta(x-x')\delta(y-y')\frac{d}{dt}\delta(t-t'). \tag{52}$$

To solve this for $t \to t'+$, it is sufficient to integrate the right side of the equation above twice with respect to t. Note that the term, $\partial_{xx} + \partial_{yy}$, can be ignored at this limit of small time during which waves do not have time to travel. This integration leads to

$$\left.\frac{\partial}{\partial t}g_r\right|_{t=t'+} = 0 \quad \text{and} \quad \mathrm{g_r} = \delta(\mathrm{x}-\mathrm{x}')\delta(\mathrm{y}-\mathrm{y}') \tag{53}$$

for $t \to t'+$. Due to this, the initial fluid velocity $\mathbf{v}$ vanishes everywhere because $H\,\mathrm{div}(\mathbf{v})$ is equal to $-\partial_t g_r$. The vanishing initial velocity ensures the integral,

$$\int_{-\infty}^{\infty} dx \int_{-\infty}^{\infty} dy g_r(t, x, y, x', y'), \tag{54}$$

will be independent of time for $t > t'$. Furthermore, the integral of g_r, $\int^t dt'' g_r(t'', x, y, t', x', y')$, is the usual retarded Green's function associated with the D'Alambertian operator in two dimensions $(\partial_{tt} - gH_0[\partial_{xx} + \partial_{yy}])$. Thus the function g_r is (see Ref. [27], p. 235)

$$\frac{1}{2\pi\sqrt{gH_{\max}}} \frac{\partial}{\partial t} \left\{ \frac{\theta[gH_{\max}(t-t')^2 - (x-x')^2 - (y-y')^2]}{\sqrt{gH_{\max}(t-t')^2 - (x-x')^2 - (y-y')^2}} \right\}, \tag{55}$$

where θ is the step function. To compute $\eta^{(i)}$ for $x = x_0^+$, one should proceed to the convolution of $s^{(i)}$ with $2g_r$ given in Eq. (55). Here the factor 2 in front of g_r stems from the fact that the sources $s^{(i)}(y)$ generate a *unit* flux exclusively towards the open ocean, while the function g_r acts in the whole space. In this convolution x and x' will both be equal to x_0 (bay mouth), and $\eta^{(i)}$ will be obtained as

$$\eta^{(i)}(t, x_0^+, y) = \int_{-\infty}^{t} dt' \int_{-Y_0}^{Y_0} dy' \frac{s^{(i)}(t', y')}{\pi\sqrt{gH_{\max}}} \frac{\partial}{\partial t} \left\{ \frac{\theta[gH_{\max}(t-t')^2 - (y-y')^2]}{\sqrt{gH_{\max}(t-t')^2 - (y-y')^2}} \right\}. \tag{56}$$

Inspecting the integral above one notices that if the time dependence of $s^{(i)}(t', y)$ is $\theta(t')$ (thus, essentially independent of time), then the integration with respect to t' can be carried out and $\eta^{(i)}$ becomes proportional to $1/t$.

Thus $\eta^{(i)}$ decays quickly for $t \gg Y_0/\sqrt{gH_{\max}}$. To sustain $\eta^{(i)}(t, x_0^+, y)$ the source, $s^{(i)}(t', y)$, must vary with time. According to the dimensional analysis $\eta^{(i)}(t, x_0^+, y)$ is of order of

$$\frac{1}{\sqrt{gH_{\max}}} t_0 \frac{\partial}{\partial t'} s^{(i)}(t', y'),$$

where t_0 is $Y_0/\sqrt{gH_{\max}}$. Taking into account $s^{(i)} \propto \sqrt{gH_{\max}}\eta^{(i-1)}$, the proportionality relation

$$\eta^{(i)} \propto \underbrace{\left(\frac{Y_0}{\sqrt{gH_{\max}}}\right)}_{t_0} \frac{\partial}{\partial t} \eta^{(i-1)} \tag{57}$$

is obtained. Therefore the series given by (50) converges rapidly if the period of the incident wave is much larger than $t_0 = Y_0/\sqrt{gH}$.

The averaged value of $\eta^{(i)}(t, x_0^+, y)$ across the width of the bay is

$$\bar{\eta}^{(i)}(t, x_0^+) = \frac{1}{2Y_0} \left(\int_{-Y_0}^{Y_0} dy \int_{-\infty}^{t} dt' \int_{-Y_0}^{Y_0} dy' \frac{s^{(i)}(t', y')}{\pi\sqrt{gH_{\max}}} \frac{\partial}{\partial t} \left\{ \frac{\theta[gH(t-t')^2 - (y-y')^2]}{\sqrt{gH_{\max}(t-t')^2 - (y-y')^2}} \right\} \right). \tag{58}$$

If the radius of the causality circle $[\sqrt{gH_{\max}}(t-t')]$ is less than $2Y_0$, then the integrand in the equation above will have severe discontinuity within the domain of integration. In general the source term,

$$s^{(i)}(t', y'),$$

is a smoother function than

$$\frac{\partial}{\partial t} \left\{ \frac{\theta[gH_{\max}(t-t')^2 - (y-y')^2]}{\sqrt{gH_{\max}(t-t')^2 - (y-y')^2}} \right\}.$$

Therefore it is preferable to proceed to the integration by parts in Eq. (58) with respect to integration variable t'. The integration by parts leads to

$$\bar{\eta}^{(1)}(t,x_0^+)=\frac{1}{2Y_0}\left(\int_{-Y_0}^{Y_0}dy\int_{-\infty}^{t}dt'\int_{-Y_0}^{Y_0}dy'\frac{\frac{\partial}{\partial t'}s^{(1)}(t',y')}{\pi\sqrt{gH_{\max}}}\left\{\frac{\theta[gH_{\max}(t-t')^2-(y-y')^2]}{\sqrt{gH_{\max}(t-t')^2-(y-y')^2}}\right\}\right), \tag{59}$$

where the identity,

$$\frac{\partial}{\partial t}g_r(t,x,y,t',x',y')=-\frac{\partial}{\partial t'}g_r(t,x,y,t',x',y'),$$

has been taken into account. Interchanging the order of integration in Eq. (59), this equation becomes

$$\bar{\eta}^{(i)}(t,x_0^+)=\frac{1}{2Y_0}\left(\int_{-\infty}^{t}dt'\int_{-Y_0}^{Y_0}dy'\int_{-Y_0}^{Y_0}dy\frac{\frac{\partial}{\partial t'}s^{(i)}(t',y')}{\pi\sqrt{gH_{\max}}}\left\{\frac{\theta[gH_{\max}(t-t')^2-(y-y')^2]}{\sqrt{gH_{\max}(t-t')^2-(y-y')^2}}\right\}\right). \tag{60}$$

Now the analytical integration with respect to y yields

$$\bar{\eta}^{(i)}(t,x_0^+)=\frac{1}{2Y_0}\left(\int_{-\infty}^{t}dt'\int_{-Y_0}^{Y_0}dy'\frac{\frac{\partial}{\partial t'}s^{(i)}(t',y')}{\pi\sqrt{gH}}\left\{\arcsin\left[\min\left(1,\frac{Y_0-y'}{\sqrt{gH}t}\right)\right]\right.\right.$$
$$\left.\left.+\arcsin\left[\min\left(1,\frac{|-Y_0-y'|}{\sqrt{gH_{\max}}t}\right)\right]\right\}\right). \tag{61}$$

We will now relate consecutive perturbative $\eta(t,x_0^+)$ terms. This can be done by eliminating the source term $s^{(i)}$ from the equation above using

$$s^{(i)}(t,y')=H(x_0,y')u^{(i-1)}(t,x_0^-)=-H(x_0,y')\sqrt{\frac{g}{\bar{H}(x_0)}}\eta^{(i-1)}(t,x_0^-), \tag{62}$$

and the sea level averaged at the mouth of the bay can be cast in the form

$$\bar{\eta}^{(i)}(t,x_0^+)=-\int_0^{+\infty}d\tau\frac{\partial}{\partial t}\eta^{(i-1)}(t-\tau,x_0^-)\Gamma(\tau), \tag{63}$$

where

$$\Gamma(\tau)=\frac{1}{2\pi\bar{H}(x_0)Y_0}\int_{-Y_0}^{Y_0}dy'\,H(x_0,y')\left\{\arcsin\left[\min\left(1,\frac{Y_0-y'}{\sqrt{gH_{\max}}\tau}\right)\right]\right.$$
$$\left.+\arcsin\left[\min\left(1,\frac{|-Y_0-y'|}{\sqrt{gH_{\max}}\tau}\right)\right]\right\}. \tag{64}$$

The expression given in Eq. (64) is valid for all types of nonreflecting bays, and by using it we can derive the relevant Γ functions for bays with parabolic, triangular, and rectangular cross sections where $\bar{H}$ is $2H/3$, $H/2$, and H, respectively. Here, of course, in triangular and rectangular bays of constant width we are referring to noninclining bathymetry, otherwise they would not be nonreflecting. The functions $\Gamma(t)$ for various geometries are displayed in Fig. 10.

If we now consider a hypothetical incident wave in the open sea with a step discontinuity given by

$$\theta[\sqrt{gH_0}t+(x-x_0)],$$

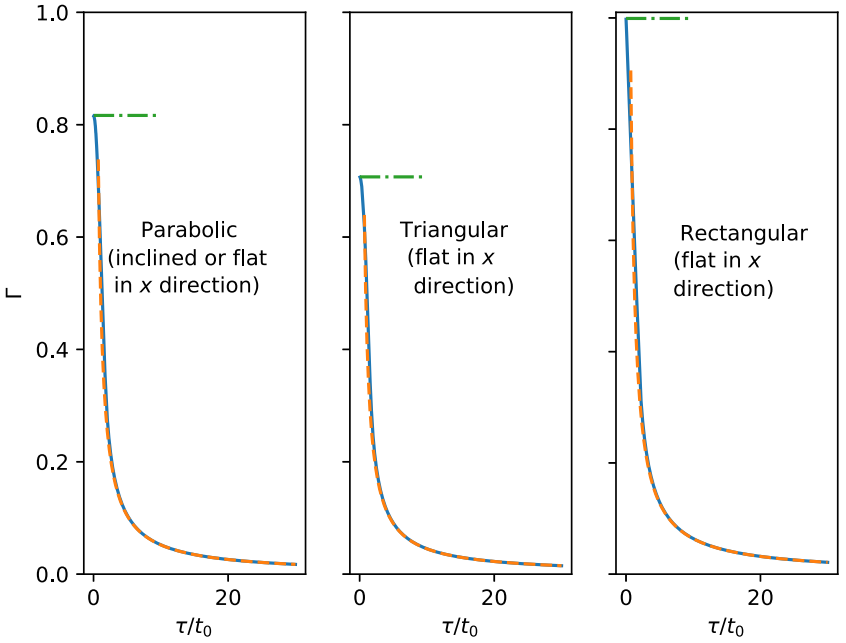

FIG. 10. The continuous curves are the function $\Gamma(\tau)$ displayed as a function of nondimensional time τ/t_0 with $t_0 = Y_0/\sqrt{gH_0}$. See (64) for the definition of Γ. The horizontal dot-dashed lines are $\sqrt{\langle H\rangle/H_0}$ [see (67)]. The dashed curves are an asymptotic approximation given by (68). For a triangular bay the depth is $H(y) = H_0(1 - |y|/Y_0)$ (depth independent of x). For a rectangular bay the depth is uniform with $H = H_0$.

then $\eta^{(0)} + \eta^{(1)}$ at $x = x_0^+$ averaged over the width of the bay will be

$$2[1 - \Gamma(t)]. \tag{65}$$

We use $\Gamma(t)$ to apply an appropriate free surface boundary condition at the bay mouth.

In the early and late stages of the diffraction, simple approximations of function $\Gamma(t)$ can be found for bays of arbitrary cross sections, long enough so that the reflection from the inland tip can be neglected. The source distribution at the mouth of such a long channel for an incident step function is

$$s^{(1)}(y) = u^{(0)}H(y) = -2\sqrt{\frac{g}{\bar{H}}}H(y).$$

At the early stage of the generation of waves by the source distribution above, the geometrical spreading of the waves in the open sea remains negligible. The solution of the one-dimensional wave equation ($\partial_{tt}\eta - gH_0\partial_{xx}\eta = 0$) for those generated by $s^{(1)}(y)$ is then

$$-2\sqrt{\frac{1}{\bar{H}H_{\max}}}H(y)\theta[\sqrt{gH_{\max}}\,t - (x - x_0)], \tag{66}$$

whose average across the mouth is equal to $-2\Gamma(t)$. Accordingly [see (65)]

$$\Gamma(t) \approx \sqrt{\frac{\bar{H}}{H_{\max}}} = \begin{cases} \sqrt{2/3} & \text{parabolic channel} \\ \sqrt{1/2} & \text{triangular channel} \\ 1 & \text{rectangular channel} \end{cases} \tag{67}$$

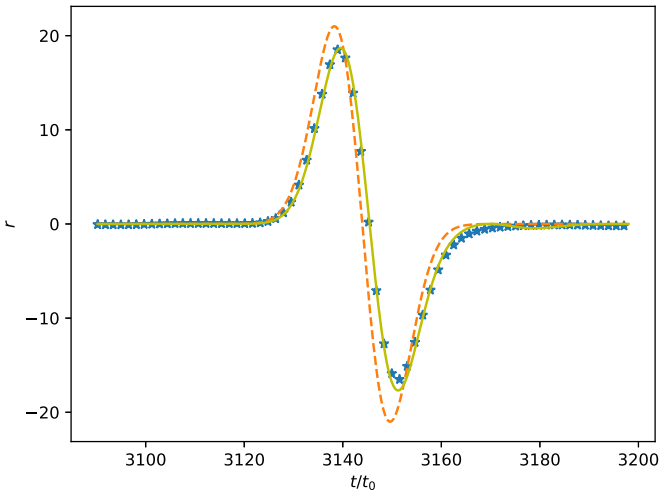

FIG. 11. Run-up generated by a Gaussian incident wave given by $\exp\{-[(x+\sqrt{gH_{\max}})(t-T/2)/(0.4x_0)]^2\}$ entering an inclined parabolic bay of aspect ratio $x_0/(2Y_0)=10$. The continuous curve is the "exact" solution found using (43), the broken curve is $r^{(0)}(t)$ (undisturbed solution of the Dirichlet problem), and the stars are $r^{(0)}(t)+r^{(1)}(t)$. The timescale t_0 is $Y_0/\sqrt{gH_{\max}}$, and T is duration of the sampling.

is obtained in the limit $t \ll W/\sqrt{gH_{\max}}$ (here W is the width of the channel). In the opposite limit $t \gg W/\sqrt{gH_{\max}}$ the function $g_r(t,x,y,t',x',y')$ can be approximated [see (55)] by

$$g_r(t,x,y,t',x',y') \approx \frac{1}{2\pi gH_{\max}}\frac{\partial}{\partial t}\left(\frac{1}{|t-t'|}\right),$$

where we neglected $y-y'$. Proceeding to convolution of the above g_r with the sources associated with the incident step function

$$\Gamma(t) \approx \frac{W}{\pi H_{\max}}\sqrt{\frac{\bar{H}}{g}}\frac{1}{t} \tag{68}$$

is found for $t \gg W/\sqrt{gH_{\max}}$. The function $\Gamma(t)$ together with these asymptotic approximations is displayed for three different geometries in Fig. 10. In Fig. 11 we show the run-up $[r^{(0)}(t))+r^{(1)}(t)$; see (51)] as displayed by stars. As seen in the figure, there is a good agreement with the "exact" solution. This perturbative approach was also applied to the bay with a rectangular shape; the results are displayed as stars in Fig. 3. In that figure the maximum normalized run-up obtained from the unperturbed Dirichlet condition, perturbative solution, and exact solution is 4.0, 3.6, and 3.52, respectively.

VI. CONCLUSION

We have shown that the problem of a wave packet entering a narrow nonreflecting bay does not require a complicated two-dimensional analysis within the bay. Furthermore, the offshore boundary condition can simply be taken as twice the amplitude of the incident wave as proposed in Ref. [7] if the wavelength of the incident wave is much larger than the width of the bay, and the solution obtained by doing so can be further improved by means of perturbations. As a geographic setting where these assumptions are valid, we can cite Ref. [13], where an incident tsunami wave with a characteristic period of around 15 minutes hit a bay in American Samoa. The wave travel time across the width of the mouth in this case was much less than 2 minutes. This strategy leads to satisfactory calculations of the maximum run-up, however, only for the timescales limited by twice

the travel time of the waves along the bay. The perturbative approach gives more accurate results for the bay with a parabolic cross section. The reason for this is that the depth is everywhere the same as the open sea across the entire width of the rectangular bay, while the parabolic bay is shallower near the edges and this causes reflections from the edges. Therefore, the free surface perturbation at the mouth is closer to twice the amplitude of the incident wave for the parabolic bay.

The perturbative approach developed in this work can be generalized to reflecting bays as long as the wavelength of the incident wave is much smaller than the length of the bay. A general width-averaged solution for waves within the bay for both reflecting nonreflecting cases can be found in Ref. [28]. In the asymptotic limit of short wavelength this solution can be seen as a superposition of incident and reflecting waves, both satisfying Green's law in the far field (near the mouth). Hence, near the mouth these are progressive waves. Because of this, there is a simple relation between the free surface perturbation and fluid velocity u, suitable for the perturbative approach.

A possible future research direction is to generalize the perturbation approach presented here to include the one-dimensional nonlinear solution provided in Ref. [16] inside the bay and handle the perturbed scattering problem using a matching scheme at various orders.

APPENDIX: GENERALIZED EIGENVALUE PROBLEM

In this Appendix we show how the regular solution of ordinary equation given by (28) can be found using a linear algebra package for the Python computer language. The emphasis will be on the easy implementation rather than the speed of computation. First, insert the series in Eq. (30) into (28). When one multiplies the resulting series by $\sqrt{2n+0.5}P_{2n}(y')$ and integrates the product from -1 to 1, a linear relation between A^{κ}_{2l}'s is found. The procedure will be repeated M times with $\sqrt{0.5}P_0(y')$, $\sqrt{2+0.5}P_2(y')$, …, $\sqrt{(2M-2)+0.5}P_{2M-2}(y')$, to get M relations between coefficients A^{κ}_{2l}. These relations can be written as

$$-\left(k^{\text{inc}}_{\text{open}}Y_0\right)^2\left(\sum_{q=0}^{2M-1}\delta_{nq}A^{\kappa}_{(2q)}\right)-\kappa^2Y_0^2\left(\sum_{q=0}^{2M-1}T_{nq}A^{\kappa}_{(2q)}\right)$$
$$+\sum_{q=0}^{2M-1}\delta_{nq}2q(2q+1)A^{\kappa}_{(2q)}=0\quad\text{for}\quad \text{n}=0,1,\ldots,\text{M}-1. \tag{A1}$$

Here $\delta_{nq}=\int_{-1}^{1}dy'\sqrt{2n+0.5}P_{2n}(y')\sqrt{2q+0.5}P_{2q}(y')$ is the Kronecker delta with $\delta_{nq}=1$ for $n=q$ and zero for $n\neq q$. The integral T_{nq} is given by

$$T_{nq}=\int_{-1}^{1}dy'\sqrt{2n+0.5}P_{2n}(y')(1-y'^2)\sqrt{2q+0.5}P_{2q}(y'). \tag{A2}$$

It is clear from the expression above that matrix $\mathbf{T}$ is a symmetrical tridiagonal matrix ($T_{ij}=0$ for $|i-j|>1$) because the Legendre polynomial of degree $2n$ is orthogonal to *all* polynomials of degree less than $2n$, and in Eq. (A2) the expression $(1-y'^2)P_{2q}(y')$ is a polynomial of degree $2(q+1)$.

Although the integrals in Eq. (A2) can be analytically calculated using a recurrence relation of Legendre polynomials it is more practical to proceed to numerical integration because these integrals should be executed only once for all frequencies.

Equation (A1) can be cast in matrix form as

$$(\kappa Y_0)^2\mathbf{T}(A_0,A_2,\ldots,A_{2M-2})^T=\mathbf{D}(A_0,A_2,\ldots,A_{2M-2})^T, \tag{A3}$$

where the superscript T denotes the transpose and $\mathbf{D}$ is a diagonal matrix with $D_{n,n}=2n(2n+1/2)-\left(k^{\text{inc}}_{\text{open}}Y_0\right)^2$. The equation above is called a generalized eigenvalue problem because the eigenvalue $(\kappa Y_0)^2$ is multiplied by the matrix $\mathbf{T}$ rather than the identity matrix. Here $\mathbf{T}$ is a positive

definite matrix because $\int_{-1}^{1} dy'(1-y'^2)f^2(y') > 0$. The usual method to transform a generalized eigenvalue problem to an ordinary eigenvalue problem without losing the symmetrical nature of matrices is to proceed with Cholesky decomposition of the positive matrix,

$$\mathbf{T} = \mathbf{S}\mathbf{S}^T,$$

where $\mathbf{S}$ is a lower triangular matrix. Defining new variables

$$(A_0^*, A_2^*, \ldots, A_{2M-2}^*)^T = \mathbf{S}^T (A_0, A_2, \ldots, A_{2M-2})^T \tag{A4}$$

and rewriting (A3) in terms of the new variables lead to

$$(\kappa Y_0)^2 \mathbf{T}\mathbf{S}^{-1^T}(A_0^*, A_2^*, \ldots, A_{2M-2}^*)^T = \mathbf{D}\mathbf{S}^{-1^T}(A_0^*, A_2^*, \ldots, A_{2M-2}^*)^T.$$

When the equation above is multiplied from left by $\mathbf{S}^{-1}$ one has an eigenvalue problem associated with a symmetrical matrix,

$$(\kappa Y_0)^2 (A_0^*, A_2^*, \ldots, A_{2M-2}^*)^T = \mathbf{S}^{-1}\mathbf{D}\mathbf{S}^{-1^T}(A_0^*, A_2^*, \ldots, A_{2M-2}^*)^T. \tag{A5}$$

The eigenvectors of the generalized eigenvalue problem can be restored multiplying eigenvectors of $\mathbf{S}^{-1}\mathbf{D}\mathbf{S}^{-1^T}$ by the matrix $\mathbf{S}^{-1^T}$. All these steps are carried out with a single call of function `linalg.eigh(D,T)` from the `scipy` package for Python. All the eigenvectors of the generalized eigenvalue problem are found with the routine `eigh`. Only the ones that conform to convergence criteria will be retained ($A_{2l} \to 0$ for $2l$ approaching M). The routine `eigh` returns eigenvalues in ascending order. In general the first half of the eigenvectors meet the convergence criteria.

To transform a generalized eigenvalue problem in Eq. (A3) it would have been easier to multiply $\mathbf{T}$ from the right and left by the diagonal matrix, $\mathbf{D}^{-1/2}$. The matrix resulting from this multiplication will be tridiagonal. We did not resort to this method because for some frequencies the matrix $\mathbf{D}$ can be singular.

[1] T. Shimozono, H. Cui, J. D. Pietrzak, H. M. Fritz, A. Okayasu, and A. J. Hooper, Short wave amplification and extreme runup by the 2011 Tohoku tsunami, Pure Appl. Geophys. **171**, 3217 (2014).

[2] H. Lamb, *Hydrodynamics* (Cambridge University Press, Cambridge, 1975).

[3] E. Bautista, F. Méndez, O. Bautista, and A. Mora, Propagation of shallow water waves in an open parabolic channel using the WKB perturbation technique, Appl. Ocean Res. **33**, 186 (2011).

[4] C. E. Synolakis, The runup of solitary waves, J. Fluid Mech. **185**, 523 (1987).

[5] G. F. Carrier, T. T. Wu, and H. Yeh, Tsunami run-up and draw-down on a plane beach, J. Fluid Mech. **475**, 79 (2003).

[6] M. Antuono and M. Brocchini, Solving the nonlinear shallow-water equations in physical space, J. Fluid Mech. **643**, 207 (2010).

[7] T. S. Stefanakis, F. Dias, and D. Dutykh, Local Run-Up Amplification by Resonant Wave Interactions, Phys. Rev. Lett. **107**, 124502 (2011).

[8] T. S. Stefanakis, S. Xu, D. Dutykh, and F. Dias, Run-up amplification of transient long waves, Q. Appl. Math. **73**, 177 (2015).

[9] A. Ezersky, D. Tiguercha, and E. Pelinovsky, Resonance phenomena at the long wave run-up on the coast, Natural Hazards Earth Syst. Sci. **13**, 2745 (2013).

[10] N. Postacioglu, M. S. Özeren, and U. Canlı, On the resonance hypothesis of storm surge and surf beat run-up, Natural Hazards Earth Syst. Sci. **17**, 905 (2017).

[11] C. Mei, *The Applied Dynamics of Ocean Surface Waves* (World Scientific, Singapore, 1992).

[12] K. Kajiura, Local behavior of tsunamis, in *Waves on Water of Variable Depth*, edited by D. Provis and R. Radok, Vol. 64 of Lecture Notes in Physics (Springer, Berlin/Heidelberg, 1977), pp. 72–79.

[13] I. Didenkulova, Tsunami runup in narrow bays: The case of Samoa 2009 tsunami, Nat. Hazards **65**, 1629 (2013).

[14] F. Løvholt, S. Glimsdal, P. Lynett, and G. Pedersen, Simulating tsunami propagation in fjords with long-wave models, Natural Hazards Earth Syst. Sci. **15**, 657 (2015).
[15] G. Pedersen, Fully nonlinear Boussinesq equations for long wave propagation and run-up in sloping channels with parabolic cross sections, Nat. Hazards **84**, 599 (2016).
[16] I. Didenkulova and E. Pelinovsky, Nonlinear wave evolution and runup in an inclined channel of a parabolic cross-section, Phys. Fluids **23**, 086602 (2011).
[17] T. Shimozono, Long wave propagation and run-up in converging bays, J. Fluid Mech. **798**, 457 (2016).
[18] D. Nicolsky, E. Pelinovsky, A. Raz, and A. Rybkin, General initial value problem for the nonlinear shallow water equations: Runup of long waves on sloping beaches and bays, Phys. Lett. A **382**, 2738 (2018).
[19] See Supplemental Material at http://link.aps.org/supplemental/10.1103/PhysRevFluids.6.034803 for a sinusoidal incident wave hitting an infinitely wide shelf.
[20] See Supplemental Material at http://link.aps.org/supplemental/10.1103/PhysRevFluids.6.034803 for a Gaussian incident wave packet hitting an infinitely shallow shelf.
[21] I. Didenkulova and E. Pelinovsky, Runup of tsunami waves in U-shaped bays, Pure Appl. Geophys. **168**, 1239 (2011).
[22] M. Abromowitz and A. Stegun, *Handbook of Mathematical Functions* (Dover, New York, 1972).
[23] E. Pelinovsky and R. K. Mazova, Exact analytical solutions of nonlinear problems of tsunami wave run-up on slopes with different profiles, Nat. Hazards **6**, 227 (1992).
[24] J. W. Miles and Y. K. Lee, Helmholtz resonance of harbours, J. Fluid Mech. **67**, 445 (1975).
[25] B. Aydın and U. Kânoğlu, Wind Set-down Relaxation, CMES-Computer Modeling in Engineering & Sciences **21**(2), 149 (2007).
[26] B. H. Choi, E. Pelinovsky, D. C. Kim, I. Didenkulova, and S.-B. Woo, Two- and three-dimensional computation of solitary wave runup on non-plane beach, Nonlinear Proc. Geophys. **15**, 489 (2008).
[27] B. Whitham, G., *Linear and Nonlinear Waves* (John Wiley and Sons, New York, 1973).
[28] N. Zahibo, E. N. Pelinovsky, V. Golinko, and N. Osipenko, Tsunami wave runup on coasts of narrow bays, Int. J. Fluid Mech. Res. **33**, 106 (2006).